
Article:
Kisembe, J., Wen, Y., Wainwright, C. et al. (Accepted: 2025) Contrasting Changes in Rainy Season Length, Rainfall Frequency, and Intensity Across Eastern Africa. Journal of Hydrometeorology. ISSN: 1525-755X (In Press)

Contrasting Changes in Rainy Season Length, Rainfall Frequency, and Intensity Across Eastern Africa

Jesse Kisembe,[a] Yixin Wen,[a] Caroline Wainwright,[b] Chris Funk,[c] Ronald I. Odongo, [a] and Weikang Qian [a]

[a] *Department of Geography, University of Florida, Gainesville, Florida*

[b] *School of Earth and Environment, University of Leeds, Leeds, United Kingdom*

[c] *Climate Hazards Center, University of California, Santa Barbara, California*

Corresponding author: Yixin Wen, yixin.wen@ufl.edu

ABSTRACT

Interannual rainfall variability presents critical challenges across eastern Africa. However, studies often focus on trends in seasonal rainfall totals, overlooking the intraseasonal characteristics that directly affect societal livelihoods. Our analysis of daily rainfall from the Climate Hazards Group Infrared Precipitation with Stations (CHIRPS) dataset (1982–2023) reveals significant and contrasting shifts across the region. In northern East Africa, the rainy season has lengthened by over a month and become wetter due to a higher frequency of rainy days. Similarly, the season in southern East Africa has lengthened by three weeks and become wetter, primarily due to rising rainfall intensity. Over the bimodal eastern Horn of Africa, the trends diverge sharply: the boreal spring "long rains" have shortened by up to a month and become drier with fewer rainy days, with intensity increasing in the southeast but decreasing in the northeast. Conversely, the boreal fall "short rains" have become longer and wetter in the northeast, while shortening and becoming drier in the southeast. Crucially, for both the long and short rains, changes in the number of rainy days are the primary factor determining seasonal totals; even where intensity has increased, it often fails to offset the decline caused by fewer rain events. These findings underscore the need for climate adaptation strategies to specifically account for sub-regional shifts in rainfall frequency and intensity. Longer dry periods between rainfall events may produce stress not represented by seasonal totals, while more intense rainfall may offer opportunities for water storage and infiltration.

1. Introduction

Most rural communities in eastern Africa depend on seasonal rains not only for agriculture (Cocking et al. 2024; Schwarzwald and Seager 2024) but also for the replenishment of groundwater wells that supply drinking water (Adloff et al. 2022). In recent years, the increasing variability of these rains has had devastating socioeconomic consequences. For example, the anomalously wet October-November-December (OND) 2019 rains (Nicholson et al. 2022) caused widespread flooding and landslides, affecting over 2 million people (Wainwright et al. 2020). Similarly, the exceptionally wet March-April-May (MAM) 2020 season led to a rapid rise in Lake Victoria’s water levels, reaching record heights and resulting in further floods and displaced populations, including those in South Sudan (Marsham 2020). In contrast, from late 2020 to late 2022, both the OND and MAM seasons were unusually dry, triggering a severe humanitarian crisis across Ethiopia, Kenya, and Somalia (IGAD Climate Prediction and Applications Center (ICPAC) 2022; Funk et al. 2023b; Kimutai et al. 2025).

Over 20 million people faced acute food insecurity due to widespread crop failures and livestock losses (ICPAC 2022; Funk et al. 2023b).

Beyond the variability in the seasonal rainfall totals, it is the increasing year-to-year fluctuations in the timing of the rainy season, as well as the distribution and intensity of individual rain events, that more directly impact societal livelihoods. For instance, consecutive seasons with delayed onsets and fewer rainy days can lead to reduced crop yields and failed harvests, posing serious threats to food security. It is therefore crucial to examine changes in these intraseasonal characteristics. Insights from such an assessment can reveal where these shifts are occurring across eastern Africa, providing essential information for developing targeted adaptation strategies and supporting the resilience of climate-vulnerable communities in the face of future climate change.

Numerous studies, based on station observations (e.g., Seleshi and Zanke 2004; Majaliwa et al. 2015; Otte et al. 2017), satellite data (e.g., Jury and Funk 2013; Funk et al. 2015b; Rowell et al. 2015; Cattani et al. 2018; Diem et al. 2019; Seregina et al. 2019; Palmer et al. 2023; Schwarzwald and Seager 2024), and local farmers' recollections (e.g., Nimusiima et al. 2013; Diem et al. 2017; Salerno et al. 2019; Yvonne et al. 2020) have documented changes in seasonal rainfall across eastern Africa. On a regional scale, studies have reported contrasting trends. For instance, Seregina et al. (2019) found a wetting trend in northern East Africa during June-July-August-September (JJAS) and in the Horn of Africa during OND over the period 1983–2013. In contrast, they observed a drying trend from November to April in southern East Africa and during MAM in the Horn. Similarly, Maidment et al. (2015) found comparable patterns in a continental-wide analysis from 1983–2010. However, the majority of these studies have primarily focused on trends in seasonal rainfall averages or totals, often defining rainy seasons by fixed calendar months. This approach overlooks the substantial spatial and temporal variability in the timing and duration of rainy seasons (Dunning et al. 2016; Seregina et al. 2019; Cocking et al. 2024). Notably, Wainwright et al. (2019) showed that the decline in MAM rains from the early 1980s to the late 2000s was associated with a shorter rainy season, marked by delayed onset and earlier cessation.

Besides, changes in seasonal rainfall totals can result from variations in both the number of rainy days and rainfall intensity (Camberlin et al. 2009; Liebmann et al. 2017). Together with the timing and duration of the rainy season, these factors, collectively referred to as intraseasonal characteristics, are key determinants of overall seasonal rainfall and play a pivotal

role in agricultural decision-making. Despite their importance, these characteristics have received relatively little attention in studies of eastern Africa. In particular, it remains unclear whether observed trends in seasonal rainfall totals are primarily due to changes in the frequency of rainy days, rainfall intensity, or a combination of both. Moreover, the spatial and temporal patterns of these intraseasonal characteristics, how they are changing over time, and where these changes are most pronounced remain poorly understood. This study addresses these gaps by asking: "Have the characteristics of the rainy seasons in eastern Africa changed in recent decades, and if so, how do these changes differ between areas with unimodal (one rainy season per year) and bimodal (two rainy seasons per year) rainfall regimes?"

Unlike many previous studies that use fixed calendar months to define rainy seasons, we employ an objective, location-specific method to determine the timing of the rainy season. This approach allows for a more accurate investigation of interannual variability based on location-specific definitions of seasonality. Using daily rainfall data from the Climate Hazards Infrared Precipitation with Stations (CHIRPS) dataset (Funk et al. 2015c), we examine changes in seasonal rainfall totals in relation to key intraseasonal characteristics: onset, cessation, rainy season length, number of rainy days, and rainy-day intensity. By decomposing the annual rainfall cycle into measures of timing, duration, amount, frequency, and intensity, we quantify how these aspects of seasonality have evolved across eastern Africa over the past four decades (1982–2023), with particular attention to differences between unimodal and bimodal rainfall regimes.

The remainder of this paper is structured as follows: Section 2 outlines the data and methods. Section 3 presents the results. Finally, Section 4 provides the discussion and conclusions, synthesizing the study's implications for understanding changes in the characteristics of the rainy seasons in eastern Africa.

2. Data and Methods

a. Rainfall data

We use the daily CHIRPS dataset, which provides rainfall estimates at a 0.05° (5 km) grid resolution from January 1, 1981, to the present. Our analysis focuses on the period 1981–2024. CHIRPS combines multiple data sources, including thermal infrared satellite imagery, direct rain gauge measurements, monthly precipitation climatology (the Climate Hazards group

Precipitation Climatology; CHPClim), and reanalysis fields from the Coupled Forecast System version 2, to generate high-resolution rainfall estimates (Funk et al. 2015c).

Researchers at the University of California, Santa Barbara have long focused on improving rainfall estimation in sub-Saharan Africa, particularly in regions with complex terrain critical for crop production. In the early 2000s, a gravity wave-based model of orographic rainfall enhancement (Funk and Michaelson 2004) was combined with interpolated station data to create the Collaborative Historical African Rainfall Model (Funk et al. 2003). Later research led to the development of advanced satellite-enhanced climatologies (Funk et al. 2015a), which enabled the CHIRPS product (Funk et al. 2015c) to capture precipitation more accurately in mountainous areas. An important aspect of the satellite-only Climate Hazards group Infrared Precipitation (CHIRP) product is its low bias compared to station data. This helps reduce spurious influences that can arise when the distribution of stations changes over time (Funk and Shukla 2022).

In East Africa, Dinku et al. (2018) compared CHIRP and CHIRPS with ARC (African Rainfall Climatology) and TAMSAT (Tropical Applications of Meteorology using SATellite and ground-based observations) products using data from 1,200 independent stations. At dekadal and monthly timescales, CHIRP and CHIRPS showed the best performance and had almost no average bias. Across Africa, CHIRPS has been shown to be resistant to spurious trends arising from changes in station distribution (Maidment et al. 2015) due to the low bias in CHIRP (Dinku et al. 2018). While all satellite-based rainfall estimates face some limitations, CHIRPS is considered the most reliable product for East Africa because it was specifically designed for the region and incorporates additional station data from meteorological agencies and other partners.

b. Classifying rainfall seasonality

The seasonality of rainfall over eastern Africa is complex and exhibits pronounced regionality (Herrmann and Mohr 2011; Lyon 2014). This complexity is largely attributed to the region's significant topographic variations (Fig. 1a) and its equatorial location (Herrmann and Mohr 2011).

To simplify this complexity, we distinguished three broad seasonality classes: areas that are dry year-round, areas with one rainy season per year (unimodal regime), and areas with two rainy seasons per year (bimodal regime).

The classification process was as follows: First, we excluded grid points with a mean annual rainfall of less than 50 mm year^{-1}, as these represent dry year-round areas with no distinct rainy season (grey areas in Fig. 1b). These areas, which are consistent with the arid seasonality class identified by Herrmann and Mohr (2011), are primarily located in the Sahara Desert, parts of Djibouti and Eritrea, the northern tip of the Horn of Africa, and the Turkana region in Kenya.

The remaining grid points were then classified as either unimodal or bimodal based on the natural logarithm of the ratio of the amplitude of the first harmonic to the amplitude of the second harmonic (Yang et al. 2015; Schwarzwald et al. 2023a). If this ratio is greater than zero, the grid point has a unimodal regime (one rainy season per year); if it's less than zero, it has a bimodal regime (two rainy seasons per year), as shown in Fig. 1b. A unimodal regime is found in the northern and southern parts of the region, while a bimodal regime is predominant east of the highlands and near the equator. The identified unimodal and bimodal regimes are consistent with findings from previous studies (Liebmann et al. 2012; Yang et al. 2015; Dunning et al. 2016; Schwarzwald et al. 2023b).

The typical seasonal rainfall cycle for each regime is shown in panels (c) to (e) of Fig. 1 for three representative countries. South Sudan and Tanzania each experience one rainy season per year, occurring during boreal summer (Fig. 1c) and boreal winter/austral summer (Fig. 1e), respectively. In contrast, Somalia experiences two rainy seasons per year (Fig. 1d), commonly referred to as the boreal spring "long rains" and boreal fall "short rains."

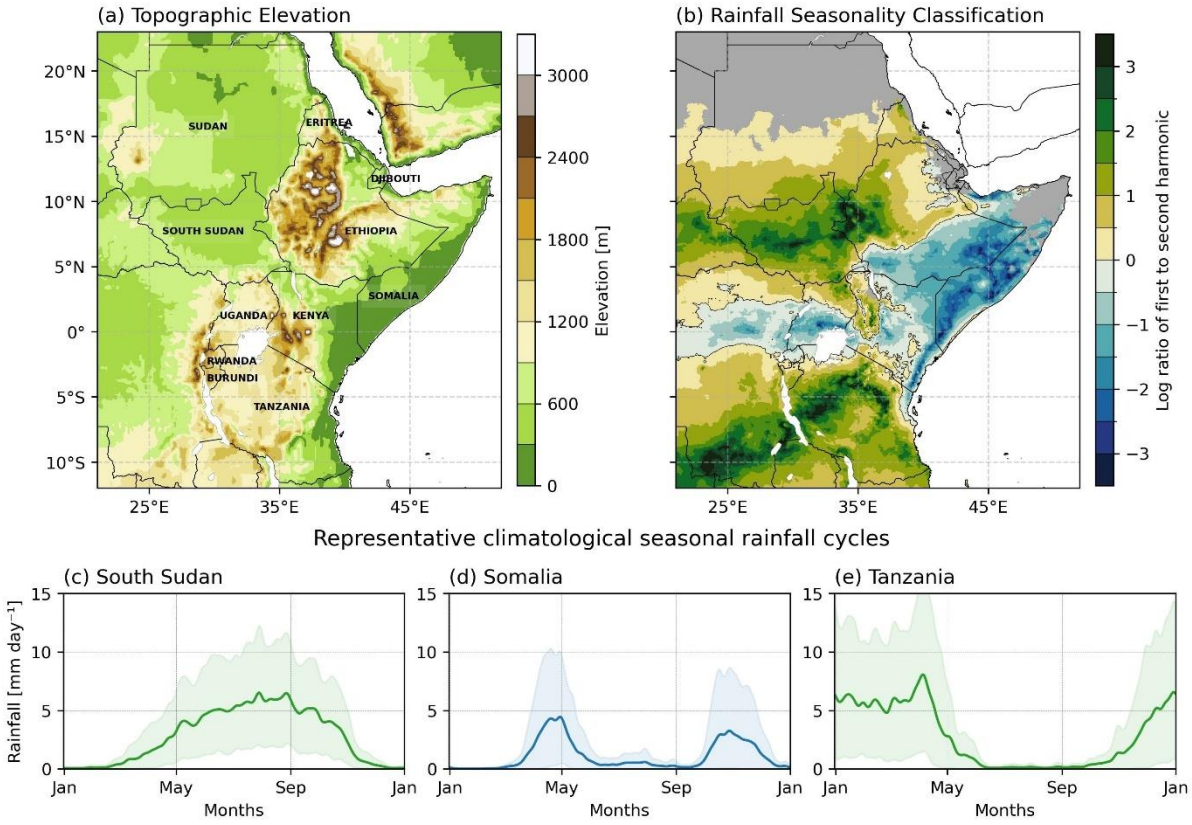

155

156 Fig. 1. Topography and rainfall seasonality of eastern Africa. (a) Elevation map of eastern
157 Africa, highlighting the 11 countries in the region. (b) Map showing the natural logarithm of
158 the ratio of the amplitude of the first harmonic to the amplitude of the second harmonic. Grey
159 shading indicates areas that are dry year-round. Panels (c)-(e) show representative
160 climatological seasonal rainfall cycles. The light-colored shading indicates the 0.1–0.9
161 interquartile range of the area-weighted average calculated across all years (1981–2024) for
162 each calendar day. The lines are smoothed using a 30-day running mean.

163 *c. Determining the onset and cessation of the rainy season*

164 The onset and cessation dates of the rainy season were determined using the anomalous
165 accumulation method of Dunning et al. (2016), which builds on the methodology originally
166 developed by Liebmann et al. (2012) for regions with a unimodal rainfall regime. Unlike
167 approaches that rely on fixed thresholds, this method defines the rainy season as the period
168 when rainfall is continuous in occurrence, duration, and intensity relative to the local
169 climatological daily mean (Diaconescu et al. 2015). By emphasizing a sustained wet period, it
170 reduces the likelihood of false onsets, that is, single heavy rainfall events followed by
171 prolonged dry spells, which can be particularly damaging to recently planted crops (Dunning
172 et al. 2016). Full methodological details are provided in Dunning et al. (2016); a summary is
173 given here.

For each grid point, the climatological wet season is determined by identifying the minima and maxima in the climatological cumulative daily rainfall anomaly, $C(d)$, calculated as:

$$C(d) = \sum_{i=1Jan}^{d} (Q_i - \bar{Q})$$

where Q_i is the climatological mean rainfall for each day d within the range of [1 Jan − 31 Dec], and $\bar{Q}$ is the climatological daily mean rainfall. The minima and maxima of $C(d)$ define the start (d_s) and end (d_e) of the climatological wet season, respectively. This calculation is performed separately for grid points with unimodal and bimodal regimes.

Next, the onset and cessation of the rainy season in each individual year are determined. For each season and year, a cumulative rainfall anomaly $A(D)$ similar to $C(d)$ above, is calculated as:

$$A(D) = \sum_{j=d_s-k}^{D} \left(R_j - \bar{Q}\right), \;\; k \in \{20, 50\}$$

where $\bar{Q}$ is the climatological daily mean rainfall (as defined as above) and R_j is the rainfall on day j. Unlike in the climatological calculation, j does not span the entire year but instead ranges from $d_s - k$ to $d_e + k$. For grid points with bimodal regime, $k = 20$; for unimodal grid points, $k = 50$. The onset date is defined as the day following the minima in $A(D)$, after which rainfall becomes persistent in occurrence, duration, and intensity (Diaconescu et al. 2015). The cessation date is the day of the maxima that follows this minima. Because some seasons can overlap into the next calendar year, as is the case in Burundi and Tanzania, we did not calculate onset and cessation dates for the first (i.e., 1981) and last (i.e., 2024) years of the dataset.

After determining the onset and cessation dates for each year, we calculated the following rainy season metrics:

- Length of the rainy season: The number of days between the onset and the cessation, which indicates the season's duration.
- Total seasonal rainfall: The sum of daily rainfall from the onset to the cessation.
- Number of rainy days: The count of days between the onset and cessation with rainfall ≥ 1 mm day^{-1}, which is indicative of the frequency of rain events. This threshold is

widely used and is an operational standard for the regional climate centre for eastern Africa, ICPAC (Gudoshava et al. 2020).

- Average rainfall per rainy day: The mean rainfall over all rainy days, which provides a measure of intensity.

d. Trend calculation

Trends in rainy season metrics were assessed using two non-parametric methods: the Theil-Sen slope estimator (Theil 1950; Sen 1968) and the Mann-Kendall test (Kendall 1938; Mann 1945). The Theil-Sen slope estimator, which is robust to outliers, calculates the trend as the median of all pairwise slopes between data points. The Mann-Kendall test then evaluates the statistical significance of these trends, with the null hypothesis being that no trend is present. Significance was assessed at the 95% confidence level ($p < 0.05$).

To quantify trend uncertainty, we applied a non-parametric bootstrap procedure alongside the Theil-Sen slope estimator. For each sub-region (Fig. 5), area-averaged annual time-series for each rainy season metric were first extracted. We then performed 10,000 bootstrap iterations, where each iteration consisted of generating a resampled series of equal length (42 years) by drawing annual values with replacement from the original record. For every resampled series, Sen's slope and intercept were recomputed, producing an ensemble of bootstrapped trend lines. The 95% confidence intervals were derived from the empirical distribution of these trend realizations, defined by the 2.5^{th} and 97.5^{th} percentiles. This non-parametric approach provides a robust, distribution-free measure of uncertainty that complements the Mann-Kendall significance test.

e. Interpretation of trend metrics

Trends are expressed in units relevant to each metric: days decade^{-1} for onset, cessation, rainy season length, and number of rainy days; mm decade^{-1} for total seasonal rainfall; and mm day^{-1} decade^{-1} for average rainfall per rainy day. A negative (positive) trend in onset or cessation indicates a shift toward an earlier (later) onset or cessation date. A positive (negative) trend in rainy season length indicates that the season is becoming longer (shorter). For the other metrics, a positive (negative) trend reflects an increase (decrease).

3. Results

a. Changes in the characteristics of the rainy season within the unimodal regime

We begin by examining areas with a unimodal regime, which is characterized by one rainy season per year. As depicted in Fig. 1b, this regime is typically found across northern and southern East Africa. Northern East Africa (NEA) encompasses areas north of the equator, including northern Uganda, northwestern Kenya, South Sudan, Sudan, Djibouti, Eritrea, and northern and western Ethiopia. Southern East Africa (SEA) refers to areas south of the equator, broadly covering parts of southern Kenya, Burundi and Tanzania.

Across NEA, on average, the onset of the rainy season progresses northward from northern Uganda in early April to northern Sudan and northern Ethiopia by mid-July (Fig. S1). In contrast, the cessation progresses southward from early September in northern Sudan, Eritrea, and Ethiopia to early November in South Sudan and northern Uganda (Fig. S1). Fig. 2a shows an earlier onset of the rainy season, with a trend of 6 days decade^{-1}, while Fig. 2b indicates a later cessation of 4 days decade^{-1}. Both trends are statistically significant across many locations within the 5ºN–15ºN latitude band. Consistent with this, climate change projections also suggest that the cessation of this rainy season will shift later by more than a week, a change linked to a slower retreat of the tropical rainband and a deepening of the Saharan heat low (Dunning et al. 2018; Wainwright et al. 2021b). The combined tendency toward a later cessation and an earlier onset suggests the dry season may be shifting later in the calendar year. Overall, the rainy season is lengthening by over 8 days decade^{-1}, a trend that is statistically significant across Sudan, western Ethiopia, eastern South Sudan, and northeastern Uganda (Fig. 2c).

Figure 2d shows a statistically significant increase in seasonal rainfall totals of 60 to more than 80 mm decade^{-1} within the 10ºN to 15ºN latitudinal band. Previous studies have also identified a coherent wetting trend across this band (Maidment et al. 2015; Seregina et al. 2019), and some of this trend likely reflects a recent recovery in rainfall following the drought conditions of the 1980s (Panthou et al. 2018; Biasutti 2019). This Sahelian rainfall recovery, which extends into NEA, has been extensively documented using multiple precipitation datasets (Nicholson 2005; Lebel and Ali 2009; Giannini 2015; Maidment et al. 2015; Sanogo et al. 2015; Nicholson et al. 2018; Panthou et al. 2018; Biasutti 2019) and satellite-observed vegetation records (Fensholt et al. 2009, 2013; Dardel et al. 2014; Pausata et al. 2020).

The increase in seasonal rainfall totals is accompanied by a significant increase in the number of rainy days, exceeding 8 days decade^{-1}, a pattern that is spatially coherent across the northern sub-region (Fig. 2e). However, the intensity of individual rainy days is decreasing, with a statistically significant decline of 0.4 to 1 mm day^{-1} decade^{-1}, particularly evident in northern Uganda, South Sudan, and northern Ethiopia (Fig. 2f). This suggests that the observed increase in seasonal rainfall totals over NEA is primarily driven by an increasing number of rainy days. It is worth noting that a distinct zone encompassing northeastern Uganda, northwestern Kenya, and southeastern South Sudan shows pronounced trends in rainy season length and total rainfall. As Herrmann and Mohr (2011) highlight, these areas are characterized by unstable rainfall seasonality with high interannual variability, and therefore, the results should be interpreted with caution.

Turning to SEA, the onset of the rainy season generally progresses eastward from Burundi in early October to central and southern Tanzania by early December (Fig. S1). In contrast, the cessation moves northward, beginning in early April in southern Tanzania and continuing to mid-May in Burundi, northern and eastern Tanzania, and parts of southern Kenya (Fig. S1). Across SEA, a trend toward an earlier onset of 4 days decade^{-1} is evident across most of the region. However, parts of southern Kenya and southern Tanzania show a contrasting trend of a later onset of 6 days decade^{-1} (Fig. 2a). A trend toward a later cessation of 6 days decade^{-1} is generally consistent across the region and is statistically significant between 10°S and 5°S (Fig. 2b). Overall, the rainy season is lengthening by 6 days decade^{-1} across most areas, except in southeastern Tanzania, where it is shortening at a similar rate (Fig. 2c). However, this trend is not statistically significant.

Total seasonal rainfall shows a statistically significant increasing trend of more than 60 mm decade^{-1}across northern, northwestern, and central Tanzania (Fig. 2d). This pattern contrasts with the declining seasonal rainfall reported by Maidment et al. (2015) and Seregina et al. (2019), indicating that seasonal rainfall has recently increased in SEA, particularly in Burundi and Tanzania. This recent increase in the unimodal rains over Tanzania has also been documented by Magang et al. (2024) and Msuya et al. (2025). Accompanying this overall increase in seasonal rainfall is a slight, but not statistically significant, change in the number of rainy days (Fig. 2e). However, the intensity of individual rainy days is increasing at a statistically significant rate of more than 1.2 mm day^{-1} decade^{-1}, particularly across Burundi and Tanzania (Fig. 2f). Notably, the spatial trend pattern of average rainfall per rainy day in

SEA closely mirrors that of total seasonal rainfall. This suggests that changes in rainfall intensity have been a key driver of the observed increase in seasonal rainfall totals, a relationship further supported by the consistency of statistically significant areas in Figs. 2d and 2f.

In summary, the rainy seasons in both NEA and SEA have lengthened and become wetter. However, the underlying causes of this increased wetness differ significantly. In NEA, the rainy season has lengthened by over 33 days (i.e., 8 days decade^{-1}), with the increase in total seasonal rainfall is primarily due to an increasing number of rainy days. In contrast, the rainy season in SEA has lengthened by 25 days (i.e., 6 days decade^{-1}), with the increase in total rainfall being largely influenced by higher rainfall intensity. This rise in intensity is often associated with an increased risk of flooding and erosion, though it can also enhance groundwater recharge, potentially increasing groundwater availability (Taylor et al. 2013; Cuthbert et al. 2019). It is also important to note a key exception: in southeastern Tanzania, an important surplus maize-producing area, the rainy season has shortened by 25 days (i.e., 6 days decade^{-1}), with its onset typically in early December and cessation in early April.

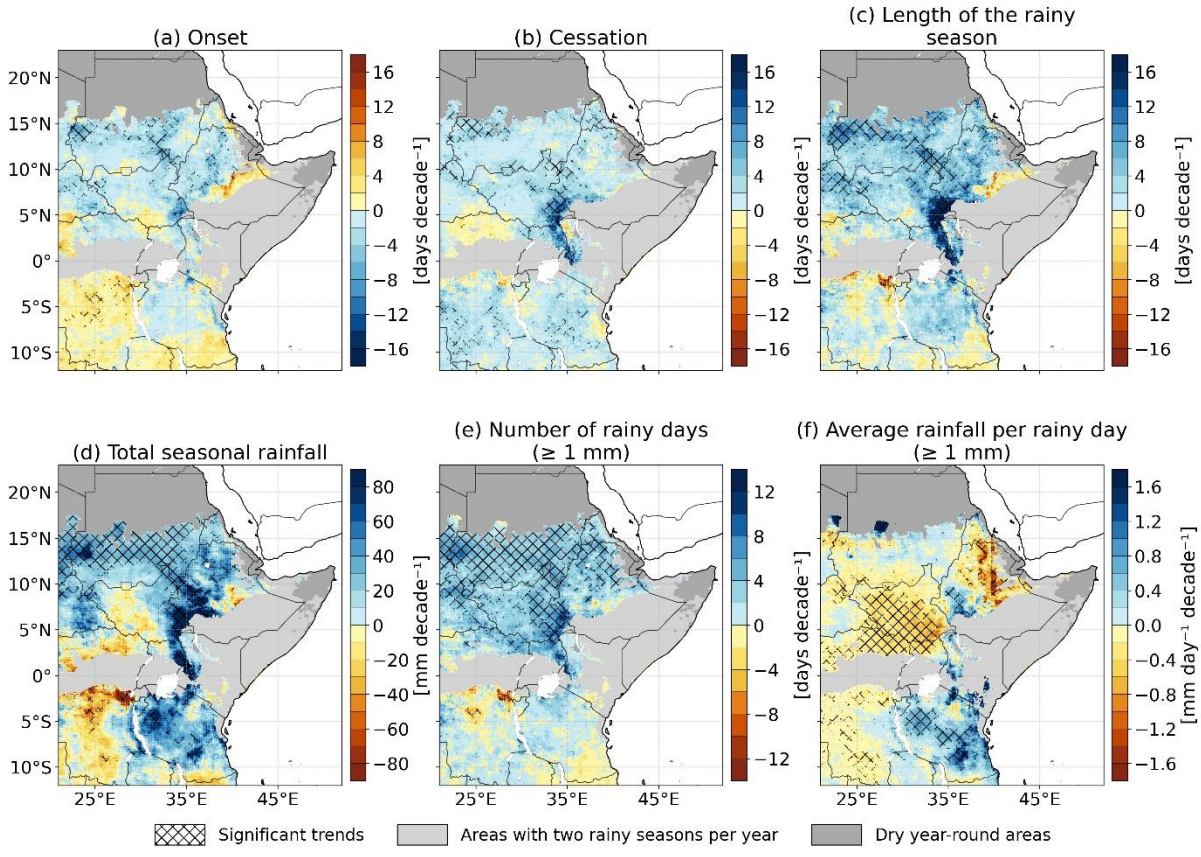

Fig. 2. Spatial trends in the characteristics of the rainy season for areas with a unimodal regime (one rainy season per year). The panels show spatial trends for (a) onset, (b) cessation, (c) rainy season length, (d) total seasonal rainfall, (e) number of rainy days, and (f) average rainfall per rainy day. Hatching indicates statistical significance at the 95% confidence level. For panels (a) and (b), a negative trend indicates a shift toward an earlier onset or cessation of the rainy season.

b. Changes in the characteristics of the rainy season within the bimodal regime

We now turn to the bimodal regime, which is characterized by two rainy seasons per year: the long rains during boreal spring and the short rains during boreal fall. As shown in Fig. 1b, this regime is typically observed across central and southern Uganda, Rwanda, parts of Tanzania, and the Horn of Africa (HoA), which includes eastern Kenya, Somalia, and southeastern Ethiopia. The discussion begins with the long rains, followed by the short rains.

1) LONG RAINS

On average, the onset of the long rains progresses northward, starting in mid-February in Rwanda and reaching late April in Somalia (Fig. S1). Cessation follows a similar northward pattern, occurring between mid- and late May, while in Kenya, the long rains typically end in late April (Fig. S1). Figure 3a shows a mixed pattern for the onset timing. A predominant trend toward an earlier onset of 4 days decade^{-1} is evident in parts of Ethiopia, Somalia, Kenya, Uganda, and northern Tanzania, with statistically significant changes west of Lake Victoria in Uganda. Conversely, a later onset of 2 to 6 days decade^{-1} is observed in isolated areas of Kenya, Somalia, Ethiopia, and northern Rwanda, though this trend is not statistically significant. Figure 3b shows a widespread trend toward an earlier cessation of the long rains, with decreases of up to 7 days decade^{-1} across much of the HoA (east of 38°E) and western Uganda. This trend is statistically significant in southeastern Ethiopia, Somalia, and coastal Kenya. These regions include important crop production areas, where an earlier cessation could have significant implications for agricultural productivity by shortening the growing season and increasing water stress for crops. In contrast, isolated areas in eastern and southwestern Uganda, western Kenya, and southwestern Ethiopia exhibit a later cessation trend of 3 days decade^{-1} (Fig. 3b), although this is not statistically significant.

The tendency toward an earlier cessation of the long rains (Fig. 3b) and earlier onset of the rainy season in NEA (Fig. 2a) suggests that the onset of the boreal summer dry season in the HoA may be shifting earlier in the calendar year. This pattern appears consistent with results

339 from Wainwright et al. (2019) and may be related to warming in the northern Indian Ocean and
340 an early start to the boreal summer Indian Monsoon circulation. The changes in onset and
341 cessation have resulted in a widespread shortening of the long rains across much of the HoA
342 (east of 38°E), with significant reductions in season length ranging from 2 to 8 days decade^{-1}
343 along the coastline (Fig. 3c). In contrast, much of Uganda, southwestern Ethiopia, and some
344 isolated areas in Kenya and Somalia show a trend toward a longer rainy season, with increases
345 exceeding 3 days decade^{-1} (Fig. 3c). This latter trend is only statistically significant in eastern
346 and southwestern Uganda.

347 Figure 3d shows a decline in seasonal rainfall totals across much of the HoA (east of 38°E),
348 ranging from 10 to over 30 mm decade^{-1}, with the exception of the Kenya-Somalia border and
349 parts of northern Somalia. This decline is collocated with the observed shortening of the rainy
350 season (Fig. 3c) and early cessation (Fig. 3b). The reduction in seasonal rainfall totals is
351 statistically significant in Ethiopia and along the HoA coastline. Consistent with these trends,
352 future climate change projections indicate continued declines in seasonal rainfall along the
353 coastline of HoA (Wainwright et al. 2021a). This has been associated with a shift in sea breeze
354 convergence further inland (Finney et al. 2020). Conversely, areas west of 38°E, including
355 southwestern Ethiopia, parts of Kenya, Uganda, and Rwanda, exhibit an increase in seasonal
356 rainfall ranging from 10 to over 40 mm decade^{-1} (Fig. 3d). This wetting trend is collocated with
357 a lengthened rainy season as shown in Fig. 3c.

358 Accompanying these rainfall changes, the number of rainy days has decreased by 1 to 3
359 days decade^{-1} across much of the HoA (Fig. 3e). This decline is statistically significant along
360 the coastline, aligning with the observed shortening of the rainy season (Fig. 3c). Conversely,
361 areas west of 38°E have experienced an increase in rainy days, ranging from 2 to 5 days decade^{-1}
362 ^{1}, with statistically significant increases in southern Uganda (Fig. 3e). The intensity of
363 individual rainy days during the long rains exhibits contrasting patterns (Fig. 3f). A significant
364 increase in average rainfall per rainy day, ranging from 0.6 to over 2.4 mm day^{-1} decade^{-1}, is
365 observed across eastern Kenya, southern Somalia, and southwestern Ethiopia. Conversely, a
366 significant decline of 0.4 to 1.8 mm day^{-1} decade^{-1} is evident in the northeastern HoA (east of
367 40°E in eastern Ethiopia and Somalia), western Uganda, and a localized area in eastern Kenya
368 (centered north and south of 40°E).

The drying trend in the long rains over the eastern HoA has been a central research focus for more than two decades. First identified by Verdin et al. (2005), this decline has since been confirmed by numerous studies using a range of precipitation datasets (Funk et al. 2005; Williams and Funk 2011; Lyon and DeWitt 2012; Liebmann et al. 2014; Lyon 2014; Lyon et al. 2014; Yang et al. 2014; Maidment et al. 2015; Rowell et al. 2015; Seregina et al. 2019; Wainwright et al. 2019; Schwarzwald and Seager 2024). Many explanations link the decline to Pacific Ocean variability (Williams and Funk 2011; Funk 2012; Lyon and DeWitt 2012; Hoell and Funk 2013; Lyon 2014; Liebmann et al. 2014, 2017; Hoell et al. 2017). Studies highlight changes in the Pacific zonal sea surface temperature (SST) gradient (Seager et al. 2019), warming in the Indo-Western Pacific SSTs, and increased convection over the Western Equatorial Pacific (Funk et al. 2018). These oceanic changes are associated with an anomalous Walker circulation over the Indian Ocean. This circulation strengthens upper-level easterlies and intensifies its descending branch. The result is increased subsidence over the eastern HoA and reduced rainfall (Williams and Funk 2011; Lyon 2014; Liebmann et al. 2014; Funk et al. 2018, 2023a, 2023b). Another explanation points to a shorter rainy season driven by regional circulation changes (Wainwright et al. 2019).

It should be noted that the hypotheses of Wainwright et al. (2019) and Funk et al. (2023a, 2023b) are not mutually exclusive. Warmer SSTs in the west Pacific, the southwestern Indian Ocean, and the northern Indian Ocean may all have contributed to the drying of the long rains. Added to these factors is a decline in the frequency of rainy days, which our results show is spatially exclusive to the eastern HoA.

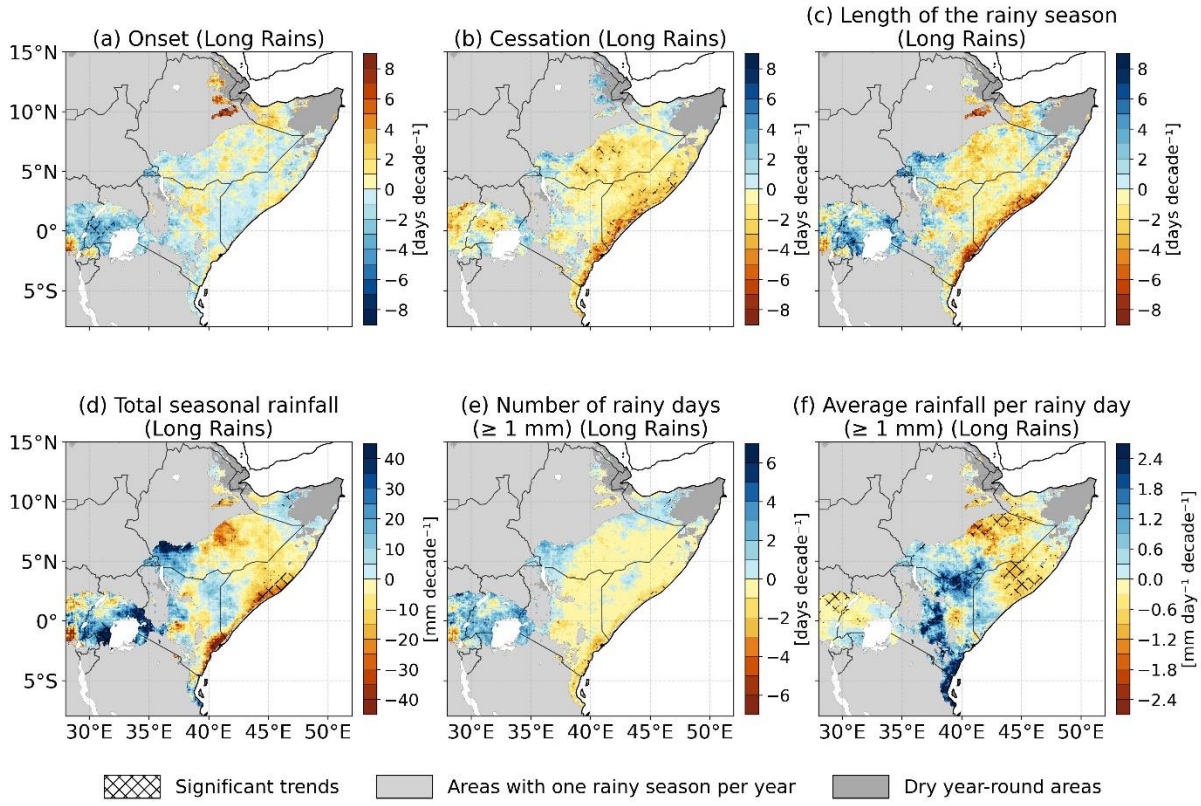

Fig. 3. Spatial trends in the characteristics of the boreal spring (long rains) season. Panels show spatial trends for (a) onset, (b) cessation, (c) rainy season length, (d) total seasonal rainfall, (e) number of rainy days, and (f) average rainfall per rainy day. Hatching indicates statistical significance at the 95% confidence level. For panels (a) and (b) a negative trend indicates a shift toward an earlier onset or cessation of the rainy season.

2) Short Rains

Regarding the short rains, the onset generally follows a southward progression, occurring between mid-July in Uganda and early October to early November in Ethiopia, Somalia, and Kenya (Fig. S1). The cessation follows a similar southward pattern, beginning in Ethiopia in mid-October and continuing until late December in Kenya and Uganda (Fig. S1). Figure 4a reveals a varied spatial pattern for onset timing. Many areas, particularly in Somalia, western and southern Ethiopia, and parts of Kenya and Uganda, show a trend toward an earlier onset, ranging from 2 to 8 days decade^{-1}. This shift is statistically significant along the Ethiopia-Kenya-Somalia border. Conversely, areas in eastern Ethiopia, eastern Kenya, and parts of western Uganda show a trend toward a later onset, ranging from 1 to 6 days decade^{-1} (Fig. 4a). In terms of cessation timing, a trend toward a later cessation of 2 to 7 days decade^{-1} is observed across the HoA, with statistical significance in much of Ethiopia and northern Somalia (Fig. 4b). An exception to this pattern is seen in eastern Kenya, where there is a tendency toward an

earlier cessation, ranging from 2 to 6 days decade^{-1}. Across much of Uganda, a later cessation trend of 2 to 4 days decade^{-1} is observed, though this trend is not statistically significant (Fig. 4b).

Similar to the later cessation of the rainy season in NEA (Fig. 2b), the trend toward a delayed cessation across much of the HoA aligns with future climate projections (Dunning et al. 2018; Wainwright et al. 2021a). This has been linked to a slower southward retreat of the tropical rainband, associated with the deepening of the Saharan heat low (Dunning et al. 2018). Overall, the trend toward a later cessation of the short rains suggests that the onset of the January-February dry season may be shifting later in the calendar year across the HoA, with Kenya as the primary exception. This has resulted into the short rains season lengthening across the HoA and Uganda (Fig. 4c). In these areas, the season has extended by 4 to over 8 days decade^{-1}, with statistically significant extensions, particularly across Ethiopia and Somalia. Conversely, eastern Kenya, parts of western Uganda, and a small region in eastern Ethiopia largely show a shortening of the season, with a trend ranging from 3 to 7 days decade^{-1}, though this trend is not statistically significant.

Compared to the long rains, the short rains show a more widespread increase in seasonal total rainfall, with trends ranging from 10 to over 40 mm decade^{-1} across the HoA and Uganda (Fig. 4d). This increase, which is statistically significant in Ethiopia, Somalia, northeastern Kenya, and eastern Uganda, coincides with a rise in the number of rainy days, with increments of 2 to 6 days decade^{-1} (Fig. 4e). Eastern Kenya presents an exception, where a drying trend of 10 to 30 mm decade^{-1} is observed. This is attributed to a shorter rainy season (Fig. 4c) and a significant reduction in the number of rainy days, which has decreased by 1 to 3 days decade^{-1} (Fig. 4e). However, when rainfall does occur in this region, it is more intense, with daily rainfall intensity significantly increasing by 1.6 to 3.2 mm day^{-1} decade^{-1} (Fig. 4f). Similar changes are observed during the long rains, indicating an overall drying trend in both seasons for eastern Kenya. Ironically, even in areas with decreasing seasonal rainfall, the increase in extreme daily rainfall intensity may potentially enhance groundwater recharge (Adloff et al. 2022).

The wetting trends observed during the short rains (Fig. 4d) align with those identified in previous studies (e.g., Liebmann et al. 2014; Maidment et al. 2015; Cattani et al. 2018; Seregina et al. 2019; Adloff et al. 2022; Palmer et al. 2023). These trends have been associated with an enhanced east-west SST gradient in the Indian Ocean, which is linked to the increasing

frequency and intensity of positive Indian Ocean Dipole (IOD) events (Liebmann et al. 2014; Dhame et al. 2020; Wainwright et al. 2020; Nicholson et al. 2022; Sun et al. 2022). Additionally, more intense El Niño events, such as those observed in 2015/16 and 2023/24, have further contributed to intense short rains.

In summary, the long and short rains in the eastern HoA show spatially contrasting changes in rainy season characteristics. In the northeastern HoA, the long rains are becoming shorter and drier, with fewer rainy days and declining rainfall intensity. Conversely, the short rains are becoming significantly longer and wetter, with more rainy days but decreasing rainfall intensity. In contrast, in the southeastern HoA, both the long and short rains are becoming significantly shorter and drier, with fewer rainy days. However, rainfall intensity in this region is significantly increasing. Overall, the long rains across the eastern HoA have shortened by 8 to 33 days (i.e., 2-8 days decade^{-1}), while the short rains have lengthened by 16 to 33 days (i.e., 4-8 days decade^{-1}). Changes in seasonal rainfall totals for both seasons are primarily driven by variations in the number of rainy days rather than changes in rainfall intensity. This is because, even in areas with increased rainfall intensity, this change does not fully offset the decline in seasonal rainfall totals caused by the decreasing number of rainy days. In the next section, we examine the interannual changes in the rainy season characteristics for selected sub-regions.

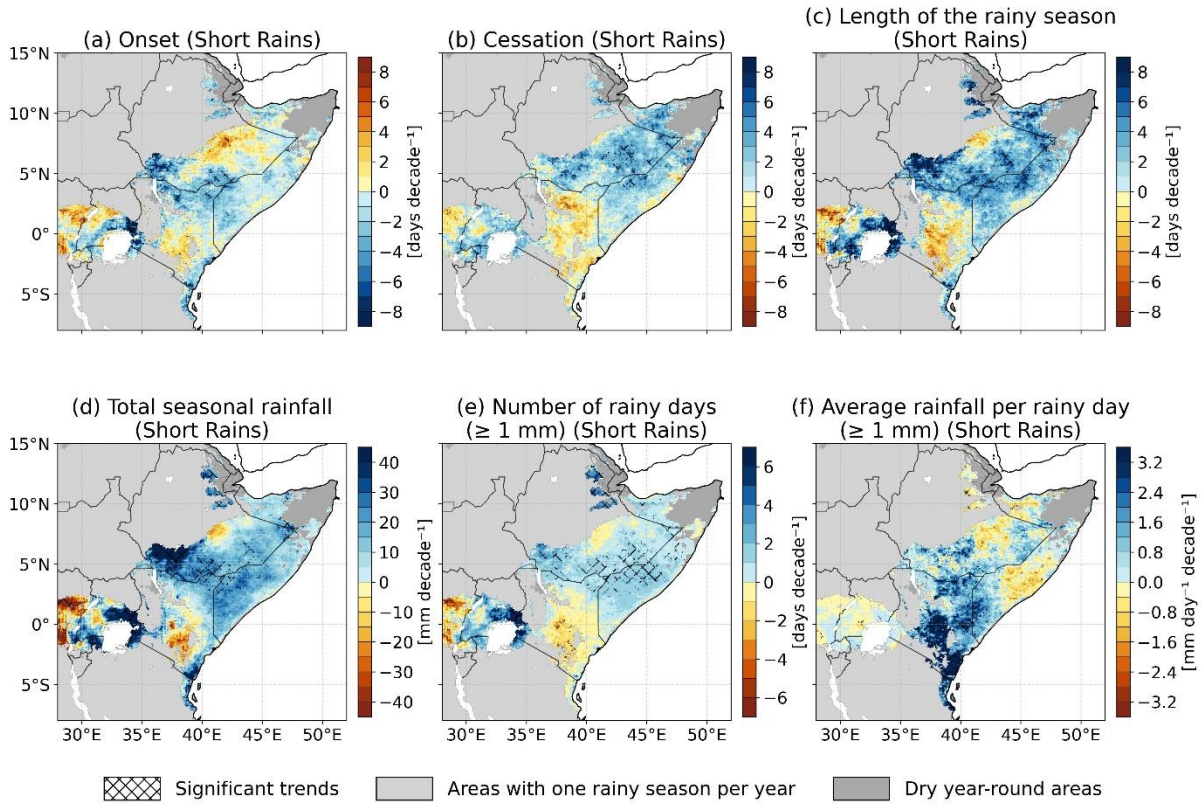

Fig. 4. As in Fig. 3, but for the boreal fall (short rains) season.

c. Interannual changes in the characteristics of the rainy seasons

To complement the spatial patterns in Figs. 2-4, we analyzed year-to-year variability to determine if the observed trends are consistent over the 1982–2023 period or if specific years disproportionately influence them. We selected four sub-regions for detailed examination (Fig. 5):

(1) Northern East Africa (NEA): Encompassing Sudan, northern Ethiopia, and southern Eritrea (10°N–15°N, 22°E–40°E), this region shows statistically significant trends in all rainy season characteristics.
(2) Northeastern Horn: This region, which covers eastern Ethiopia and central Somalia (2°N–7°N, 43°E–48°E), exhibits statistically significant trends in total seasonal rainfall during both the long and short rains.
(3) Southeastern Horn: Located in eastern Kenya (2°S–1°N, 37°E–40°E), this region shows a drying trend in both the long and short rains, with a statistically significant increase in average rainfall per rainy day.
(4) Southern East Africa (SEA): This region, located in Burundi and Tanzania (8°S–3°S, 30°E–38°E), exhibits significant trends in average rainfall per rainy day.

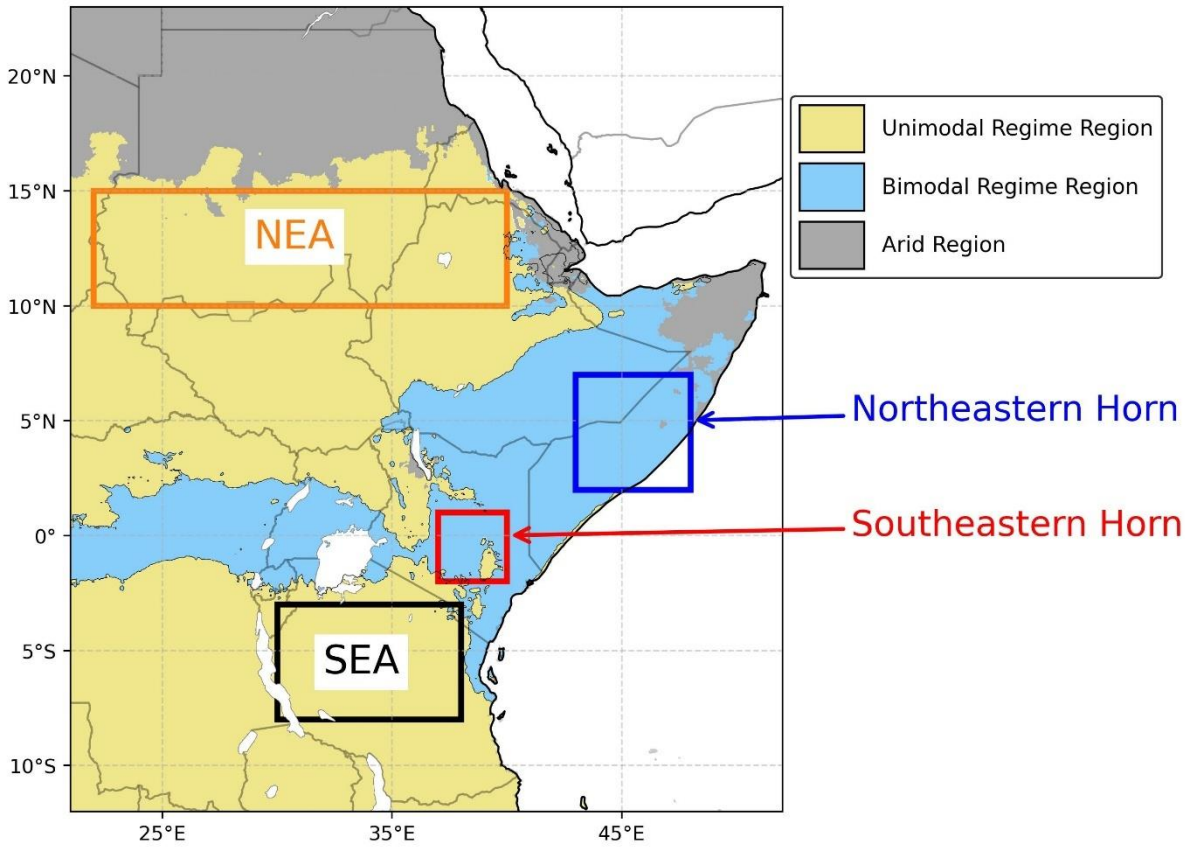

475

476 Fig. 5. Regions used for analyzing interannual changes in the rainy season characteristics.
477 The figure delineates NEA (Northern East Africa), SEA (Southern East Africa), and the
478 Northeastern and Southeastern Horn subregions to highlight areas with notable changes.
479 Background shading indicates unimodal, bimodal, and arid rainfall regimes, consistent with
480 the classification shown in Fig. 1b.

481 We separately analyzed these regions by comparing the interannual changes in four key
482 metrics: rainy season length, total seasonal rainfall, number of rainy days, and the average
483 rainfall per rainy day. A consolidated numerical summary of the regional trend magnitudes for
484 these four metrics is provided in Supplementary Table S1. The interannual changes in the onset
485 and cessation dates are shown in Figures S2-S7. The discussion begins with the two regions
486 under the unimodal regime and concludes with those in the bimodal regime.

487 1) NORTHERN EAST AFRICA

488 Over NEA, the rainy season has significantly lengthened, with a trend of 4.31 days decade^{-1}
489 during 1982–2023 (Fig. 6a). This lengthening is accompanied by significant increases in total
490 seasonal rainfall (27.88 mm decade^{-1}; Fig. 6b) and number of rainy days (3.52 days^{-1} decade^{-1};
491 Fig. 6c). By contrast, the average rainfall per rainy day has significantly declined by 0.22 mm

492 day^{-1} decade^{-1} (Fig. 6d). The robustness of these trends is confirmed as the 95% confidence
493 intervals do not overlap zero in any case. Part of the observed increase in seasonal rainfall is
494 likely related to the recent recovery of rainfall in the West African Sahel at similar latitudes
495 following the severe droughts of the 1980s (Biasutti 2019), as well as influences from decadal
496 climate variability (Maidment et al. 2015; Pausata et al. 2020).

497 Upon examining the time-series in Figure 6b, a distinct pattern emerges: a drier period from
498 1982 to 1992, followed by a gradual rainfall recovery starting in 1993, despite significant year-
499 to-year variability. The early drier period was marked by shorter rainy seasons (9 seasons out
500 of 11 seasons) with fewer rainy days (10 seasons out of 11), though with increasing rainfall
501 intensity (7 seasons out of 11). In contrast, the period since 1993 has seen longer rainy seasons
502 with a greater number of rainy days, though with decreasing rainfall intensity.

503 This recent increase in seasonal rainfall has contributed to the greening of the Sahel-
504 Sudanian zone (Dardel et al. 2014; Pausata et al. 2020), but it has also led to devastating
505 consequences. Since 2017, and especially following the exceptional 2019 OND rains, recurring
506 seasonal riverine floods have impacted South Sudan's Bahr el Ghazal and Greater Upper Nile
507 provinces. These floods have displaced thousands, damaged infrastructure, and inundated
508 croplands, triggering severe humanitarian crises (Relief and Rehabilitation Commission (RRC)
509 2023).

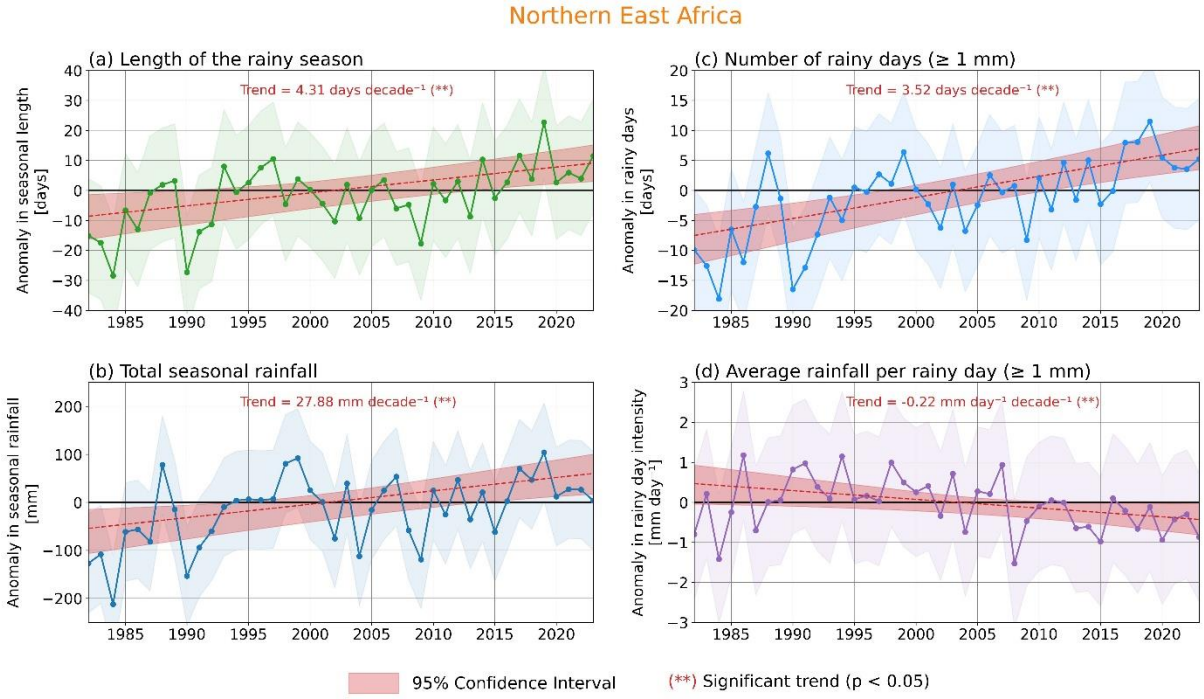

510

Fig. 6. Time-series of (a) rainy season length, (b) total seasonal rainfall, (c) the number of rainy days, and (d) average rainfall per rainy day over Northern East Africa. Interannual anomalies are shown as solid lines and are computed relative to the 1991-2020 baseline. The shaded envelope around each time series represents the standard deviation of that metric across the region for each year. The red dotted line denotes the linear trend estimated using the Theil-Sen slope estimator, and the red shaded area represents the 95% confidence interval derived from the non-parametric bootstrap procedure (see methods section). Statistically significant trends ($p < 0.05$) are marked with double asterisks (**).

2) SOUTHERN EAST AFRICA

In SEA, only the increase in rainfall intensity (0.42 mm day^{-1} $decade^{-1}$; Fig. 7d) is statistically significant. While the rainy season has lengthened by 3.63 days $decade^{-1}$ (Fig. 7a) and both total seasonal rainfall (40.33 mm $decade^{-1}$; Figure 7b) and the number of rainy days at (1.17 $days^{-1}$ $decade^{-1}$; Fig. 7c) have risen, these trends are not significant as their 95% confidence intervals overlap zero.

A closer look at Figure 7b reveals a drier period spanning from the early 1980s to the early 2010s, followed by a shift to a wetter period. The drier period, particularly from 1990 to 2014, was marked by shorter rainy seasons with fewer rainy days of lower intensity. This era included notable droughts, such as the prolonged 1998–2005 event, which led to widespread crop failures, livestock losses, and reduced water reservoir levels (Kijazi and Reason 2009). Since 2015, the region has entered a wetter period with longer rainy seasons, accompanied by an increase in the number of rainy days and rainfall intensity. The marked rise in average rainfall per rainy day since 2015 has significantly contributed to the overall increase in total seasonal rainfall over SEA, despite only a modest rise in the number of rainy days.

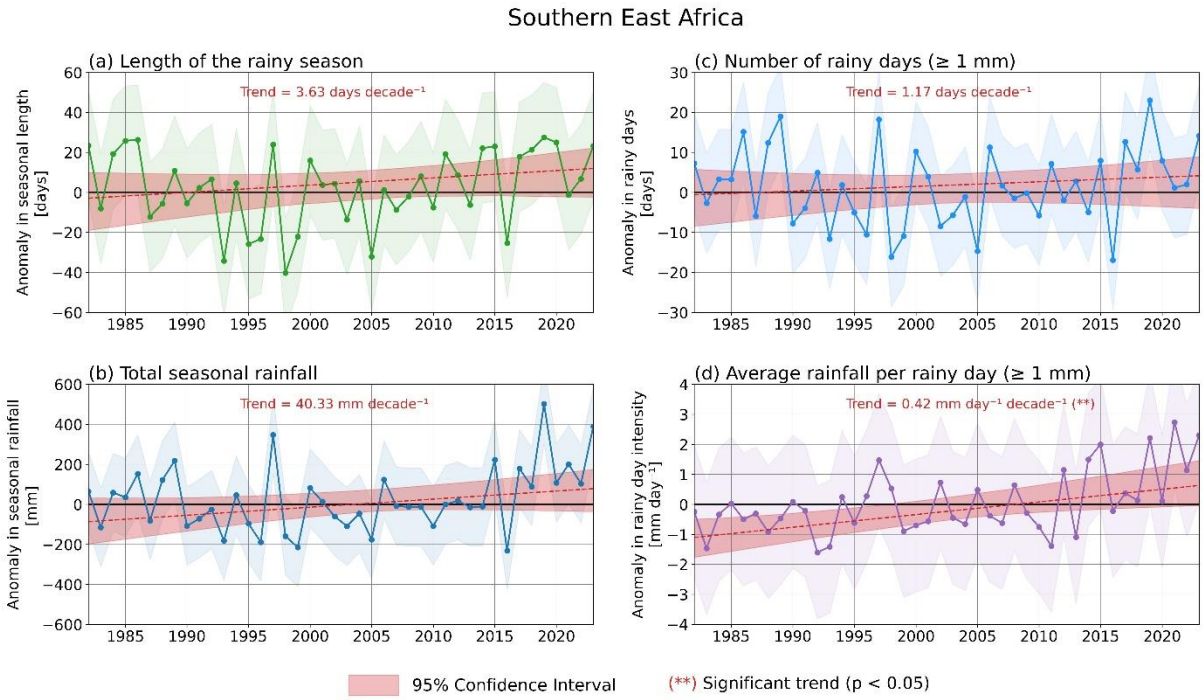

Fig. 7. As in Fig. 6, but for (a) rainy season length, (b) total seasonal rainfall, (c) the number of rainy days, and (d) average rainfall per rainy day over Southern East Africa.

3) EASTERN HORN OF AFRICA

Figures 3 and 4 show that in the eastern HoA, the long rains and short rains have contrasting trends in average rainfall per rainy day. Rainfall intensity has increased in the southeast and decreased in the northeast. This contrast forms the basis for dividing the eastern HoA into two distinct regions, which we will now discuss.

For the long rains in both the southeastern and northeastern Horn, trends in most rainy season characteristics are not statistically significant, as their 95% confidence intervals overlap with zero. The exception to this is average rainfall per rainy day. In both regions, the rainy season has shortened, with a trend of 0.58 days decade^{-1} in the southeast (Fig. 8a) and 1.02 days decade^{-1} in the northeast (Figure 9a). This shorter rainy season is accompanied by a decline in total seasonal rainfall, with a trend of 3.67 mm decade^{-1} in the southeast (Fig. 8c) and 9.94 mm decade^{-1} in the northeast Fig. 9c). This decline is primarily associated with fewer rainy days (0.50 days^{-1} decade^{-1} in the southeast, Fig. 8e; 0.56 days^{-1} decade^{-1} in the northeast, Fig. 9e). Rainfall intensity, however, shows contrasting patterns: it has significantly increased in the southeast (0.98 mm day^{-1} decade^{-1}; Fig. 8g) but has significantly declined in the northeast (0.60 mm day^{-1} decade^{-1}; Fig. 9g). Despite the rise in intensity in the southeastern Horn, it does not offset the reduction in rainy days, which ultimately leads to an overall decline in long rains

554 rainfall totals. Total seasonal rainfall and the number of rainy days appear to be in phase,
555 indicating that seasonal rainfall totals may be more influenced by the frequency of rainy days.
556 The decline in the long rains is consistent with the changes in the season length noted by
557 Wainwright et al. (2019). Our findings expand on this by showing the decline is also
558 accompanied by a reduction in the number of rainy days. This may have implications for
559 agriculture, since more frequent dry days can stress crops.

560 For the short rains, all metrics in both regions are not statistically significant, as their 95%
561 confidence intervals overlap zero, except for rainfall intensity in the southeastern Horn. In the
562 southeastern Horn, total seasonal rainfall has declined by 7.78 mm decade^{-1} (Fig. 8d), a trend
563 accompanied by a significant reduction in rainy days (1.26 days decade^{-1}; Fig. 8f) and a
564 significant increase in rainfall intensity (3.41 mm day^{-1} decade^{-1}; Fig. 8h). This tendency toward
565 higher short rains rainfall intensities could increase the risks of flooding and erosion but also
566 provide opportunities for water retention and management (Adloff et al. 2022). In the
567 northeastern Horn, the rainy season length (3.29 days decade^{-1}; Fig. 9b), total seasonal rainfall
568 (13.27 mm day^{-1} decade^{-1}; Fig. 9d), and number of rainy days (1.15 days decade^{-1}; Fig. 9f) all
569 show increasing trends, while rainfall intensity has decreased by 0.23 mm day^{-1} decade^{-1} (Fig.
570 9h). Similar to the long rains, the frequency of rainy days appears to be the primary driver of
571 total seasonal rainfall in both regions.

572 It is worth noting that focusing solely on trends can over-emphasize the impact of a few
573 wet years and obscure shifts in water stress. A striking observation is therefore related to shifts
574 in the frequencies of below-normal rainy season metrics between the 1982–1998 era and the
575 1999–2023 period. Despite several wet recent seasons in the long rains (2018, 2020, 2023) and
576 short rains (2019, 2023), there is a shift towards more frequent drier conditions in the
577 southeastern Horn (Fig. 8). In the 25 years since 1999, only 10 (40%) of the long rains seasons
578 and 9 (36%) of the short rains seasons were longer than average. Similarly, only 9 (36%) of
579 the long rains seasons and 7 (28%) of the short rains seasons received above-normal rainfall.
580 This trend extends to the number of rainy days, with only 9 seasons in both the long and short
581 rains after 1999 having more than the average number of rainy days. These shifts are likely
582 related to a drying tendency associated with stronger Pacific SST gradients and Walker
583 Circulation intensification (Funk et al. 2023b; Schwarzwald and Seager 2024).

584 A review of the time-series for the northeastern Horn (Fig. 9), reveals a marked divergence
585 in the frequency of above-normal outcomes between the long and short rains since 1999. The

long rains have shown a consistent tendency toward being shorter, drier, and less intense. Only 9 (36%) seasons have had above-normal rainfall. 12 (48%) seasons were longer than average, only 10 (25%) seasons had more than average number of rainy days, and just 6 (24%) seasons experienced above-normal rainfall intensity on rainy days. The short rains, on the other hand, appear to have become substantially and significantly longer, with greater total rainfall, a higher number of rainy days, and higher rainfall intensities. More than half the seasons were longer than average, and 11 (44%) seasons had above-normal rainfall, a higher number of rainy days, and above-normal rainfall intensity on rainy days.

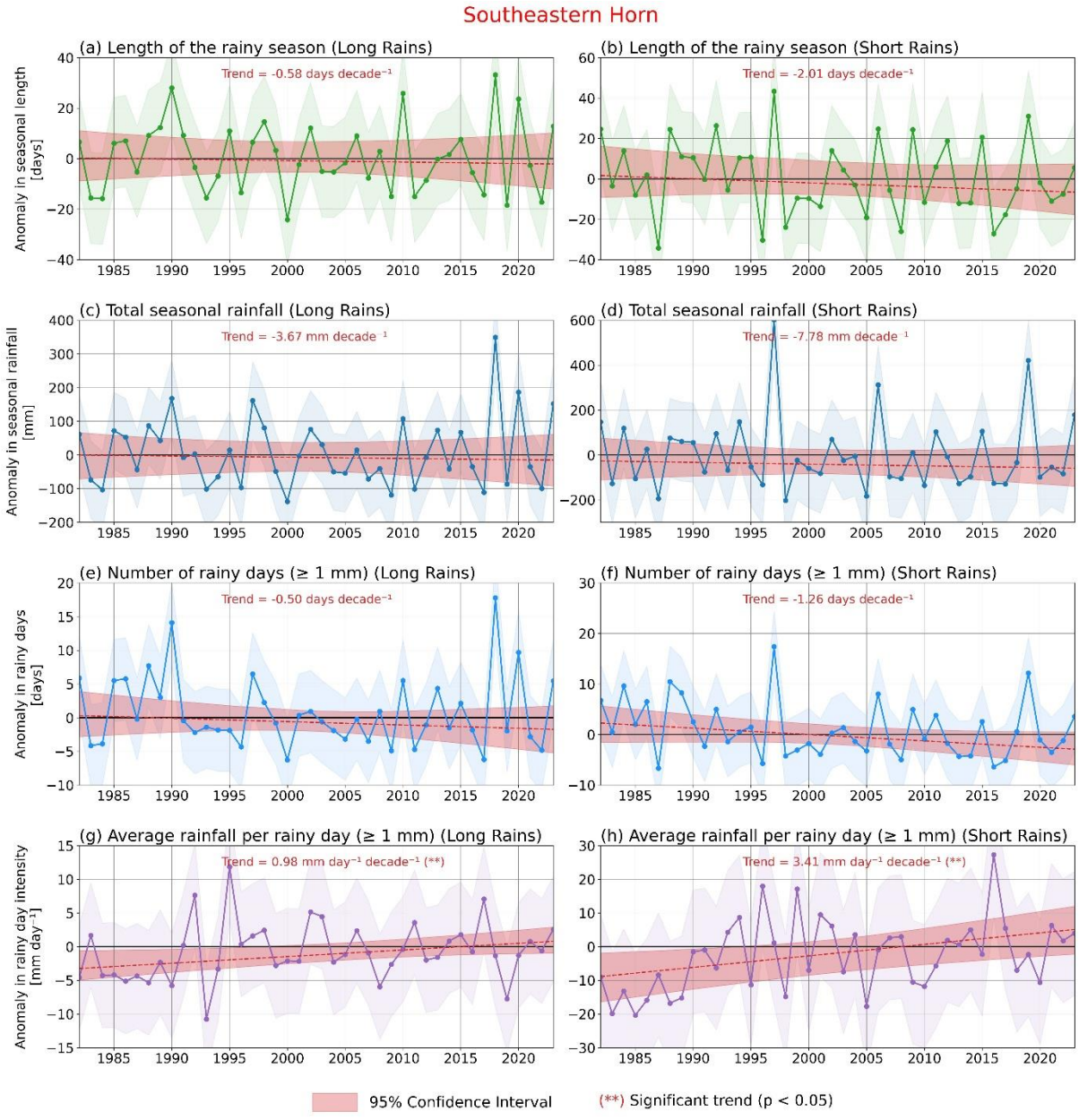

Fig. 8. As in Fig. 6, but for the long rains (left panel) and short rains (right panel) over the southeastern Horn. Panels show time-series for (a, b) rainy season length, (c, d) total seasonal rainfall, (e, f) number of rainy days, and (g, h) average rainfall per rainy day.

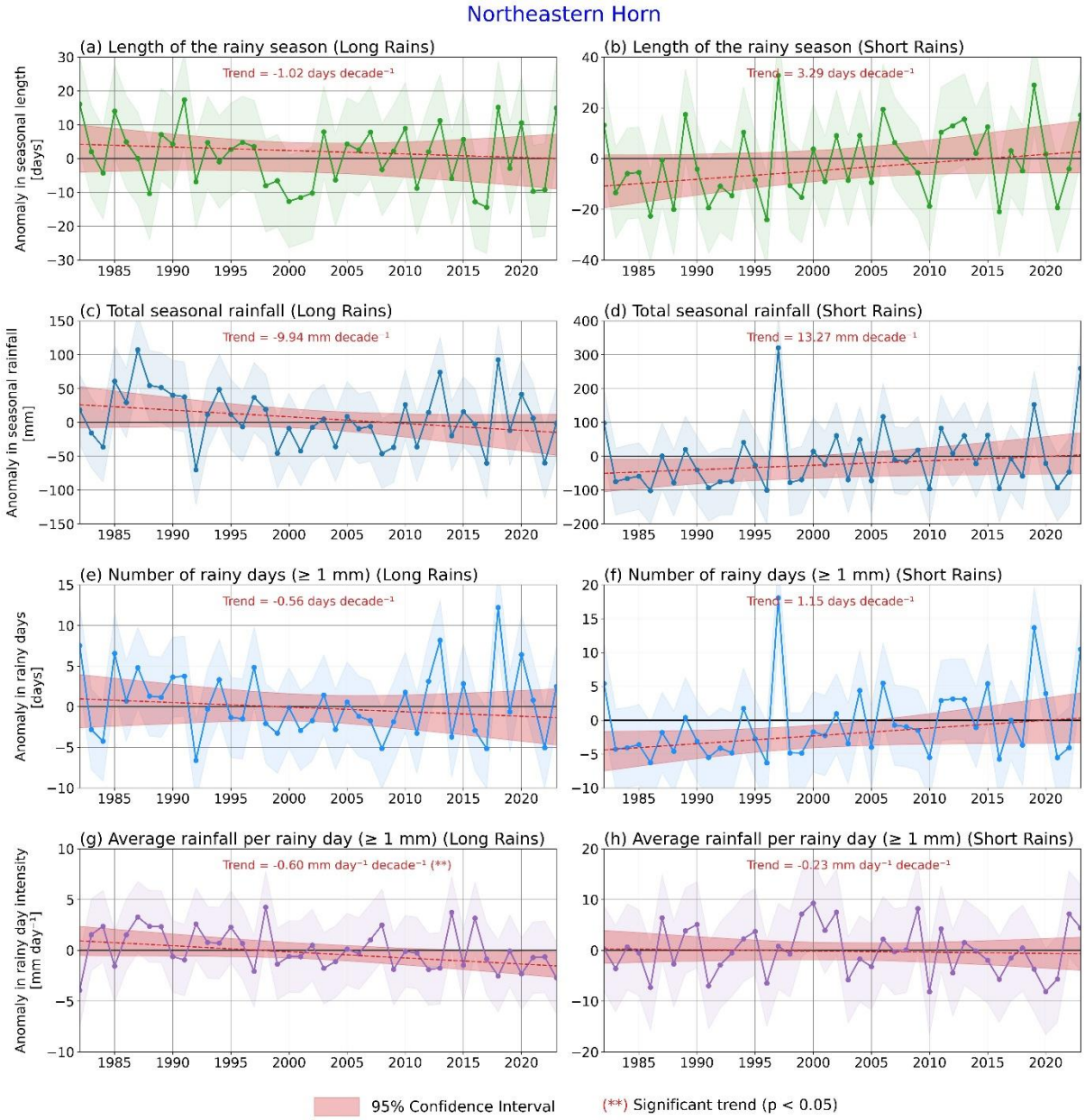

Fig. 9. As in Fig. 6, but for the long rains (left panel) and short rains (right panel) over the northeastern Horn. Panels show time-series for (a, b) rainy season length, (c, d) total seasonal rainfall, (e, f) number of rainy days, and (g, h) average rainfall per rainy day.

4. Discussion and Conclusions

Whereas previous studies across eastern Africa have largely examined seasonal rainfall totals in isolation, our analysis links these totals with the intraseasonal characteristics that shape them. This approach reveals contrasting trends in rainy season characteristics both within and

between unimodal and bimodal rainfall regimes, from which we draw the following conclusions:

- The rainy seasons in both northern and southern East Africa have lengthened and become wetter. The season in the north has extended by over a month, while that in the south has extended by more than three weeks. However, the underlying drivers of these changes differ. In the north, the increase in seasonal rainfall totals is mainly due to a higher frequency of rainy days. In contrast, in the south, the increase in rainfall is largely a result of rising rainfall intensity.
- The long rains season in the eastern HoA has become shorter and drier. The season has shortened by a range of one week to over a month, with fewer rainy days overall. However, the intensity of individual rainy days shows a contrasting pattern: it has significantly increased in the southeastern Horn but decreased in the northeastern Horn.
- The short rains season shows contrasting patterns in the eastern HoA. In the northeastern Horn, the short rains have significantly lengthened (by over two weeks to more than a month) and become wetter, accompanied by an increase in the number of rainy days. Conversely, in the southeastern Horn, the short rains have shortened (by more than three weeks) and become drier. This is accompanied by an increase in rainfall intensity, even as the number of rainy days decreases.
- Changes in seasonal rainfall totals for both the long and short rains are primarily due to variations in the number of rainy days rather than changes in rainfall intensity. This is because in areas like southeastern Horn, where rainfall intensity has increased, this increase does not fully offset the decline in seasonal rainfall totals that results from having fewer rainy days.
- A changing seasonal pulse in the annual north–south progression of East African rains is apparent. Specifically, the observed shortening of the long rains appears consistent with both the lengthening of the southern unimodal rainy season and the earlier onset of the northern unimodal rainy season. Additionally, the lengthening of the northern unimodal rainy season aligns with the earlier onset of the short rains, collectively signaling to a broader regional shift in the timing of seasonal rainfall.

These findings are based on the CHIRPS dataset, which has limitations: it relies solely on geostationary thermal infrared satellite observations, which cannot directly sense hydrometeors and precipitation, and is further affected by sparse and declining observation networks.

638 However, CHIRPS is less likely to produce spurious trends (Maidment et al. 2015) due to the
639 inherent low bias in CHIRP (Dinku et al. 2018). Despite these limitations, which are present
640 not only in CHIRPS but also in other satellite-based precipitation estimates, confidence in our
641 main findings is supported by numerous prior studies focused on seasonal rainfall trends.

642 The strength of the trends identified in this study are moderate and we have presented them
643 as moderately conclusive. It is not surprising that many 0.05° grid cells do not show
644 significance at this fine spatial resolution, given that many factors can influence precipitation
645 within such a grid cell. For this reason, areas of non-significance should be interpreted
646 cautiously. However, while confidence at the grid scale is low, it may increase when results
647 are summarized over homogeneous areas. Additionally, a more detailed, process-level
648 understanding of these results should also enhance confidence.

649 Caution is also warranted when interpreting results for transition zones (i.e., the boundary
650 between unimodal and bimodal rainfall regimes) and humid areas such as the Lake Victoria
651 Basin, which are important agricultural regions. In these areas, the anomalous accumulation
652 method is less reliable due to year-to-year shifts in the seasonal cycle. As Herrmann and Mohr
653 (2011) note, such regions are characterized by unstable rainfall seasonality with high
654 interannual variability.

655 The interannual variability of seasonal rainfall totals is modulated by changes in the
656 intraseasonal characteristics of the rainy season. In individual years, anomalously wet or dry
657 conditions can result from different combinations of factors, including variations in season
658 length, the number of rainy days, and rainfall intensity per rainy day, a finding consistent with
659 Camberlin et al. (2009). Although the influence of major climate modes (e.g., El Niño Southern
660 Oscillation (ENSO) and IOD) on interannual rainfall variability in eastern Africa is well
661 documented (Nicholson 2017; Palmer et al. 2023; Cai et al. 2025), further research is needed
662 to characterize their effects on sub-seasonal rainfall frequency and intensity. For instance, El
663 Niño and positive IOD events are known to enhance rainfall during the short rains, but do they
664 lead to more rainy days or to higher or lower rainfall intensities? In practice, seasonal outlooks
665 from ICPAC (https://www.icpac.net/seasonal-forecast/) are often framed in terms of above- or
666 below-normal seasonal rainfall totals. Yet from a societal perspective, it is not the seasonal
667 totals but the frequency and intensity of rainfall events that most affect livelihoods. Addressing
668 this question can provide valuable insights for improving sub-seasonal forecasting products

669 and help societies better prepare for future wet or dry seasons. Interestingly, the links suggested
670 here between seasonal rainfall totals and the frequency of rainy days may indicate opportunities
671 for prediction. If seasonal rainfall can be predicted, presumably the number of rainy days may
672 also be forecast effectively.

673 Over the eastern HoA, both the long and short rains exhibit a characteristic drying trend in
674 eastern Kenya. This decline is marked by a decreasing number of rainy days coupled with a
675 significant increase in rainfall intensity on days when it does rain. This pattern, which combines
676 fewer rainy days with more intense rain events, is likely the result of several overlapping
677 physical processes. The general expectation is that warm air holds more water vapor, leading
678 to increased rainfall intensity on rainy days. Supporting this, spatial maps showing substantial
679 signals along higher elevation areas near the coast might suggest orographic processes may be
680 interacting with changes in atmospheric stability and water vapor to concentrate the available
681 moisture into fewer, heavier rainfall events. Additionally, eastern Kenya lies under the
682 descending Indian Ocean branch of the Walker Circulation, and the strengthening of this
683 branch suppresses rainfall (Hastenrath et al. 2010; Funk et al. 2023b) by increasing static
684 stability over eastern East Africa (Schwarzwald et al. 2023b). This region is also influenced by
685 multiple teleconnections, including ENSO, the IOD, the Madden-Julian Oscillation (MJO), and
686 warming in the west Pacific. For instance, an increased frequency of La Niña events
687 particularly double La Niñas, can suppress rainfall in subsequent long rains seasons due to
688 sustained changes in SSTs in the tropical Pacific Ocean (Anderson et al. 2023). Additionally,
689 warming of the tropical Indo-Pacific Warm Pool intensifies the thermodynamic forcing of the
690 Walker Circulation, contributing to drier long rains seasons over eastern East Africa (Funk et
691 al. 2023b). While these links remain to be rigorously quantified, developing a clearer
692 understanding of how such large-scale drivers interact with orographic processes could provide
693 opportunities for improved seasonal forecasts.

694 While this study attributes some of the observed trends to remote teleconnections,
695 separating natural variability from anthropogenic influences would be an interesting and
696 necessary extension. Previous detection-attribution studies (e.g., Funk et al. 2018, 2019, 2023b;
697 Kimutai et al. 2025) already suggest that anthropogenic climate change has significantly
698 contributed to the drying of the long rains in eastern East Africa. For future work, a systematic
699 attribution of changes to different drivers is needed to clarify whether recent trends result from
700 natural or anthropogenic forcing, and to what extent common mechanisms explain current and

future changes. In particular, simulations from the Detection and Attribution Model Intercomparison Project (DAMIP, part of CMIP6; Gillett et al. 2016) could provide clearer attribution of these observed changes. At present, the declines in the long rains are thought to arise from an interaction of climate and natural variability, related to the relative warming of the western Pacific compared to the equatorial eastern Pacific. Funk et al. (2023b) provide explicit CMIP6-based attribution analyses for western and eastern Pacific SSTs. The western Pacific is clearly dominated by a very strong externally-forced warming trend. However, the eastern Pacific, in observations, has been characterized by a lack of warming, which is at odds with the CMIP6 projections. As discussed in Funk et al. (2023b) and Seager et al. (2019), this discrepancy may relate to model deficiencies, an extremely strong episode of natural decadal variability, or some combination of the two.

The changes documented here, together with increasing year-to-year variability, have significant implications for societal livelihoods across eastern Africa. Alterations in rainy season length and increasingly erratic rainfall undermine agricultural planning and reduce crop yields (Diem et al. 2019; Ahmed 2023; Ahmed et al. 2025). Rising rainfall intensity also heightens flood risks in both urban and rural areas, though through different ways (Douglas 2017; Gebrehiwot 2018; Ahmed et al. 2025). On a positive note, higher rainfall intensities may enhance groundwater recharge in drylands (Taylor et al. 2013; Cuthbert et al. 2019), providing a potential buffer against seasonal rainfall deficits (Adloff et al. 2022). Variations in season length may likewise offer opportunities to adjust cropping calendars, crop choices, and water management strategies to better align with the changing rainfall seasonality.

In closing, it is important to note that ongoing efforts are being made to build climate-resilient communities within the region. For example, a collaborative initiative involving the Kenya Meteorological Department, PlantVillage, Shamba Shape Up, and the Climate Hazards Center provides text and television-based advisories to rural communities in Kenya to help them manage climate shocks. However, in the face of future climate change, adaptive strategies will need to be comprehensive, prioritizing current impacts while anticipating the expected ones. Studies of historical shifts, such as those presented here, can help climate service providers “close the last mile” (Baylis et al. 2025) and provide trusted and actionable information.

Acknowledgments.

We express our gratitude to the three anonymous reviewers for their excellent suggestions, which significantly improved the manuscript. The authors (Jesse Kisembe, Yixin Wen, Ronald Inguula Odongo, and Weikang Qian) were supported by the College of Liberal Arts and Sciences at the University of Florida.

Data Availability Statement.

The CHIRPS daily rainfall dataset (Funk et al., 2015c) is available from the Climate Hazards Group at the University of California, Santa Barbara, and can be accessed at their repository: https://data.chc.ucsb.edu/products/CHIRPS-2.0/global_daily/netcdf/p05/.

REFERENCES

Adloff, M., M. B. Singer, D. A. MacLeod, K. Michaelides, N. Mehrnegar, E. Hansford, C. Funk, and D. Mitchell, 2022: Sustained water storage in Horn of Africa drylands dominated by seasonal rainfall extremes. *Geophys. Res. Lett.,* **49**, e2022GL099299, https://doi.org/10.1029/2022GL099299

Ahmed, A., 2023: Effects of Rainfall Variability on Maize Production in Afgooye District, Lower Shebelle Region, Somalia. Asian *Journal of Research in Crop Science,* **8**, 167, https://doi.org/10.9734/ajrcs/2023/v8i3167

Ahmed, S. M., A. A. Ibrahim, F. A. Farah, and A. H. Nur, 2025: Impact of Rainfall Variations on the Production of Major Crops: Sorghum (Sorghum bicolor) and Maize (Zea mays) in Burao District, Somaliland. *AgroEnvironmental Sustainability*, **3**, 64-76, https://doi.org/10.59983/s2025030108

Anderson, W., B. I. Cook, K. Slinski, K. Schwarzwald, A. McNally, and C. Funk, 2023: Multiyear La Niña events and multiseason drought in the Horn of Africa. *J. Hydrometeor.,* **24**, 119-131, https://doi.org/10.1175/JHM-D-22-0043.1

Baylis, K., and Coauthors, 2025: Five lessons for closing the last mile: How to make climate decision support actionable. *Earth's Future*, **13**, e2024EF005799. https://doi.org/10.1029/2024EF005799

Biasutti, M., 2019: Rainfall trends in the African Sahel: Characteristics, processes, and causes. *Wiley Interdiscip.* Rev.: *Climate Change,* **10**, e591, https://doi.org/10.1002/wcc.591

Cai, W., and Coauthors, 2025: Climate impacts of the El Niño–Southern Oscillation in Africa. *Nat. Rev. Earth Environ.,* **6**, 503-520, https://doi.org/10.1038/s43017-025-00705-7

764 Camberlin, P., V. Moron, R. Okoola, N. Philippon, and W. Gitau, 2009: Components of rainy
765 seasons' variability in Equatorial East Africa: onset, cessation, rainfall frequency and
766 intensity. *Theor. Appl. Climatol.,* **98**, 237-249, https://doi.org/10.1007/s00704-009-0113-
767 1

768 Cattani, E., A. Merino, J. A. Guijarro, and V. Levizzani, 2018: East Africa rainfall trends and
769 variability 1983–2015 using three long-term satellite products. *Remote Sens.,* **10**, 931,
770 https://doi.org/10.3390/rs10060931

771 Cocking, K., and Coauthors, 2024: Locally defined seasonal rainfall characteristics within the
772 Horn of Africa drylands from rain gauge observations. *J. Hydrometeor.,* **25**, 1845-1861,
773 https://doi.org/10.1175/JHM-D-23-0228.1

774 Cuthbert, M. O., and Coauthors, 2019: Observed controls on resilience of groundwater to
775 climate variability in sub-Saharan Africa. *Nature*, **572**, 230-234,
776 https://doi.org/10.1038/s41586-019-1441-7

777 Dardel, C., L. Kergoat, P. Hiernaux, E. Mougin, M. Grippa, and C. J. Tucker, 2014: Re-
778 greening Sahel: 30 years of remote sensing data and field observations (Mali, Niger).
779 *Remote Sens. Environ.,* **140**, 350-364, https://doi.org/10.1016/j.rse.2013.09.011

780 Dhame, S., A. S. Taschetto, A. Santoso, and K. J. Meissner, 2020: Indian Ocean warming
781 modulates global atmospheric circulation trends. *Climate Dyn.,* **55**, 2053-2073,
782 https://doi.org/10.1007/s00382-020-05369-1

783 Diaconescu, E. P., P. Gachon, J. Scinocca, and R. Laprise, 2015: Evaluation of daily
784 precipitation statistics and monsoon onset/retreat over western Sahel in multiple data
785 sets. *Climate Dyn.*, **45**, 1325-1354, https://doi.org/10.1007/s00382-014-2383-2

786 Diem, J. E., J. Hartter, J. Salerno, E. McIntyre, and A. Stuart Grandy, 2017: Comparison of
787 measured multi-decadal rainfall variability with farmers' perceptions of and responses to
788 seasonal changes in western Uganda. *Reg. Environ. Change*, **17**, 1127-1140,
789 https://doi.org/10.1007/s10113-016-0943-1

790 Diem, J. E., H. S. Sung, B. L. Konecky, M. W. Palace, J. Salerno, and J. Hartter, 2019: Rainfall
791 characteristics and trends—and the role of Congo westerlies—in the western Uganda
792 transition zone of equatorial Africa from 1983 to 2017. *J. Geophys. Res. Atmos.,* **124**,
793 10712-10729, https://doi.org/10.1029/2019JD031243

794 Dinku, T., C. Funk, P. Peterson, R. Maidment, T. Tadesse, H. Gadain, and P. Ceccato, 2018:
795 Validation of the CHIRPS satellite rainfall estimates over eastern Africa. *Quart. J. Roy.*
796 *Meteor. Soc.,* **144**, 292-312, https://doi.org/10.1002/qj.3244

797 Douglas, I., 2017: Flooding in African cities, scales of causes, teleconnections, risks,
798 vulnerability and impacts. *International Journal of disaster risk reduction*, **26**, 34-42,

https://doi.org/10.1016/j.ijdrr.2017.09.024

Dunning, C. M., E. C. Black, and R. P. Allan, 2016: The onset and cessation of seasonal rainfall over Africa. *J. Geophys. Res. Atmos.,* **121**, 11405-11424, https://doi.org/10.1002/2016JD025428

Dunning, C. M., E. Black, and R. P. Allan, 2018: Later wet seasons with more intense rainfall over Africa under future climate change. *J. Climate,* **31**, 9719-9738, https://doi.org/10.1175/JCLI-D-18-0102.1

Fensholt, R., K. Rasmussen, P. Kaspersen, S. Huber, S. Horion, and E. Swinnen, 2013: Assessing land degradation/recovery in the African Sahel from long-term Earth observation based primary productivity and precipitation relationships. *Remote Sens.* **5**, 664-686, https://doi.org/10.3390/rs5020664

Fensholt, R., K. Rasmussen, T. T. Nielsen, and C. Mbow, 2009: Evaluation of earth observation based long term vegetation trends—intercomparing NDVI time series trend analysis consistency of Sahel from AVHRR GIMMS, Terra MODIS and SPOT VGT data. *Remote Sens. Environ.,* **113***,* 1886-1898, https://doi.org/10.1016/j.rse.2009.04.004

Finney, D. L., J. H. Marsham, D. P. Rowell, E. J. Kendon, S. O. Tucker, R. A. Stratton, L. S. Jackson, 2020: Effects of explicit convection on future projections of mesoscale circulations, rainfall, and rainfall extremes over Eastern Africa. *J. Climate*, **33**, 2701-2718, https://doi.org/10.1175/JCLI-D-19-0328.1

Funk, C. C. 2012: Exceptional warming in the western Pacific-Indian Ocean warm pool has contributed to more frequent droughts in eastern Africa. *Bull. Amer. Meteor. Soc.*, **93**, 1049-1051, https://doi.org/10.1175/BAMS-D-12-00021.1

Funk, C., A. H. Fink, L. Harrison, Z. Segele, H. S. Endris, G. Galu, D. Korecha, and S. Nicholson, 2023b: Frequent but predictable droughts in East Africa driven by a Walker circulation intensification. *Earth's Future,* **11**, e2022EF003454, https://doi.org/10.1029/2022EF003454

Funk, C., and Coauthors, 2019: Examining the Potential Contributions of Extreme "Western V" Sea Surface Temperatures to the 2017 March–June East African Drought. *Bull. Amer. Meteor. Soc.*, **100**, S55–S60, https://doi.org/10.1175/BAMS-D-18-0108.1

Funk, C., and Coauthors, 2018: Examining the role of unusually warm Indo-Pacific sea-surface temperatures in recent African droughts. *Quart. J. Roy. Meteor. Soc.,* **144**, 360-383, https://doi.org/10.1002/qj.3266

Funk, C., and Coauthors, 2023a: Tailored forecasts can predict extreme climate informing proactive interventions in East Africa. *Earth's Future*, **11***,* e2023EF003524, https://doi.org/10.1029/2023ef003524

834 Funk, C., and J. Michaelsen, 2004: A simplified diagnostic model of orographic rainfall for
835 enhancing satellite-based rainfall estimates in data poor regions. *J. Appl. Meteor.*, **43**,
836 1366-1378, https://doi.org/10.1175/JAM2138.1

837 Funk, C., J. Michaelsen, J. Verdin, G. Artan, G. Husak, G. Senay, H. Gadain, and T. Magadzire,
838 2003: The collaborative historical African rainfall model: description and evaluation. *Int.*
839 *J. Climatol.,* **23**, 47-66, https://doi.org/10.1002/joc.866

840 Funk, C., S. E. Nicholson, M. Landsfeld, D. Klotter, P. Peterson, and L. Harrison, 2015b: The
841 centennial trends greater horn of Africa precipitation dataset. *Sci. Data,* **2**, 150050,
842 https://doi.org/10.1038/sdata.2015.50

843 Funk, C., and Coauthors, 2015c: The climate hazards infrared precipitation with stations-a new
844 environmental record for monitoring extremes. *Sci. Data,* **2**, 150066,
845 https://doi.org/10.1038/sdata.2015.66

846 Funk, C., and Coauthors, 2005: In F. NET (Ed.), *Recent drought tendencies in Ethiopia and*
847 *equatorial-subtropical eastern Africa. Vulnerability to food insecurity: Factor*
848 *Identification and characterization report* (Vol. 12). US Agency for International
849 Development.

850 Funk, C., and S. Shukla, 2020: *Drought Early Warning and Forecasting: Theory and Practice*.
851 Elsevier Press, 238 pp.

852 Funk C., A. Verdin, J. Michaelsen, P. Peterson, D. Pedreros, and G. Husak, 2015a: A global
853 satellite-assisted precipitation climatology, *Earth Syst. Sci. Data*, **7**, 275-287,
854 https://doi.org/10.5194/essd-7-275-2015

855 Gebrehiwot, K. A., 2018: A review on waterlogging, salinization and drainage in Ethiopian
856 irrigated agriculture. *Sustain. Water Resour. Manag.,* **4**, 55-62,
857 https://doi.org/10.1007/s40899-017-0121-8

858 Giannini, A., 2015: Climate change comes to the Sahel. *Nature Clim. Change*, **5**, 720-721,
859 https://doi.org/10.1038/nclimate2739

860 Gillett, N. P., H. Shiogama, B. Funke, G. Hegerl, R. Knutti, K. Matthes, and C. Tebaldi, 2016:
861 The detection and attribution model inter comparison project (DAMIP v1. 0) contribution
862 to CMIP6. *Geoscientific Model Development*, **9**, 3685-3697, https://doi.org/10.5194/gmd-
863 9-3685-2016

864 Gudoshava, M., and Coauthors, 2020: Projected effects of 1.5º C and 2º C global warming
865 levels on the intra-seasonal rainfall characteristics over the Greater Horn of Africa.
866 *Environ. Res. Lett.,* **15**, 034037, https://doi.org/10.1088/1748-9326/ab6b33

867 Hastenrath, S., D. Polzin, and C. Mutai, 2010: Diagnosing the droughts and floods in equatorial
868 East Africa during boreal autumn 2005–08. *J. Climate*, **23**, 813-817,

https://doi.org/10.1175/2009JCLI3094.1

Herrmann, S. M., and K. I. Mohr, 2011: A continental-scale classification of rainfall seasonality regimes in Africa based on gridded precipitation and land surface temperature products. *J. Appl. Meteor. Climatol.,* **50**, 2504-2513, https://doi.org/10.1175/JAMC-D-11-024.1

Hoell, A., and C. Funk, 2013: Indo-Pacific sea surface temperature influences on failed consecutive rainy seasons over eastern Africa. *Climate Dyn.,* **43**, 1645-1660, https://doi.org/10.1007/s00382-013-1991-6

Hoell, A., M. Hoerling, J. Eischeid, X. W. Quan, and B. Liebmann, 2017: Reconciling theories for human and natural attribution of recent East Africa drying. *J. Climate,* **30**, 1939-1957, https://doi.org/10.1175/JCLI-D-16-0558.1

ICPAC, FEWS-NET, WMO, FAO, WFP, and JRC, 2022: Unprecedented drought brings threat of starvation to millions in Ethiopia, Kenya, and Somalia. https://knowledge4policy.ec.europa.eu/publication/unprecedented-drought-brings-threat-starvation-millions-ethiopia-kenya-somalia_en

Jury, M. R., and C. Funk, 2013: Climatic trends over Ethiopia: regional signals and drivers. *Int. J. Climatol.,* **33**, 1924-1935, https://doi.org/10.1002/joc.3560

Kendall, M. G., 1938: A New Measure of Rank Correlation. *Biometrika,* **30**, 81, https://doi.org/10.2307/2332226

Kijazi, A. L., and C. J. C. Reason, 2009: Analysis of the 1998 to 2005 drought over the northeastern highlands of Tanzania. *Climate Res.,* **38**, 209-223, https://doi.org/10.3354/cr00784

Kimutai, J., and Coauthors, 2025: Human-induced climate change increased 2021-2022 drought severity in Horn of Africa. *Wea. Climate Extremes*, **47**, 100745, https://doi.org/10.1016/j.wace.2025.100745

Lebel, T., and A. Ali, 2009: Recent trends in the central and western Sahel rainfall regime (1990–2007). *J. Hydrology,* **375**, 52-64, https://doi.org/10.1016/j.jhydrol.2008.11.030

Liebmann, B., I. Bladé, C. Funk, D. Allured, X. W. Quan, M. Hoerling, A. Hoell, P. Peterson, and W. M. Thiaw, 2017: Climatology and interannual variability of boreal spring wet season precipitation in the eastern Horn of Africa and implications for its recent decline. *J. Climate,* **30**, 3867-3886, https://doi.org/10.1175/JCLI-D-16-0452.1

Liebmann, B., I. Bladé, G. N. Kiladis, L. M. Carvalho, G. B. Senay, D. Allured, S. Leroux, and C. Funk, 2012: Seasonality of African precipitation from 1996 to 2009. *J. Climate,* **25**, 4304-4322, https://doi.org/10.1175/JCLI-D-11-00157.1

Liebmann, B., M. P. Hoerling, C. Funk, I. Bladé, R. M. Dole, D. Allured, X. Quan, P. Pegion, and J. K. Eischeid, 2014: Understanding recent eastern Horn of Africa rainfall variability and change. *J. Climate,* **27**, 8630-8645, https://doi.org/10.1175/JCLI-D-13-00714.1

Lyon, B., 2014: Seasonal drought in the Greater Horn of Africa and its recent increase during the March–May long rains. *J. Climate,* **27**, 7953-7975, https://doi.org/10.1175/JCLI-D-13-00459.1

Lyon, B., A. Barnston, and D. G. DeWitt, 2014*:* Tropical Pacific forcing of a 1998–99 climate shift: Observational analysis and climate model results for the boreal spring season. *Climate Dyn.*, **43**, 893-909, https://doi.org/10.1007/s00382-013-1891-9

Lyon, B., and D. G. DeWitt, 2012: A recent and abrupt decline in the East African long rains. *Geophys. Res. Lett.,* **39**, https://doi.org/10.1029/2011GL050337

Magang, D.S., M. A. Ojara, L. Yunsheng, and P. H. King'uza, 2024: Future climate projection across Tanzania under CMIP6 with high-resolution regional climate model. *Sci. Rep.,* **14**, 12741, https://doi.org/10.1038/s41598-024-63495-w

Maidment, R. I., R. P. Allan, and E. Black, 2015: Recent observed and simulated changes in precipitation over Africa. *Geophys. Res. Lett.,* **42**, 8155-8164, https://doi.org/10.1002/2015GL065765

Mann, H. B., 1945: Nonparametric Tests Against Trend. *Econometrica,* **13**, 245–259, https://doi.org/10.2307/1907187

Majaliwa, J. G. M., and Coauthors, 2015: Characterization of historical seasonal and annual rainfall and temperature trends in selected climatological homogenous rainfall zones of Uganda. *Global J. Sci. Res.,* **15**, 21-40, http://oar.icrisat.org/id/eprint/10818

Marsham, J., 2020: East Africa faces triple crisis of Covid-19, locusts and floods. Accessed 7 May 2025, https://water.leeds.ac.uk/news/east-africa-faces-triple-crisis-of-covid-19-locusts-and-floods/

Msuya, O. H., Z. Yu, and S. d. Semgomba, 2025: Analysis of Spatiotemporal Trends and Variability in Precipitation Extremes over Tanzania during 1981-2023. *J. Geosci. Environ. Protection*, ***13***, 156-177, https://doi.org/10.4236/gep.2025.131009

Nicholson S., 2005: On the question of the "recovery" of the rains in the West African Sahel. *Journal of Arid Environments,* **63**, 615-641, https://doi.org/10.1016/j.jaridenv.2005.03.004

Nicholson, S. E., 2017: Climate and climatic variability of rainfall over eastern Africa. *Rev. Geophys.,* **55**, 590-635, https://doi.org/10.1002/2016RG000544

936 Nicholson S. E., A. H. Fink, and C. Funk, 2018: Assessing recovery and change in West
937 Africa's rainfall regime from a 161-year record. *Int. J. Climatol.,* **38**, 3770-3786,
938 https://doi.org/10.1002/joc.5530

939 Nicholson, S. E., A. H. Fink, C. Funk, D. A. Klotter, and A. R. Satheesh, 2022: Meteorological
940 causes of the catastrophic rains of October/November 2019 in equatorial Africa. *Global*
941 *Planetary Change*, **208**, 103687, https://doi.org/10.1016/j.gloplacha.2021.103687

942 Nimusiima, A., C. P. K. Basalirwa, J. G. M. Majaliwa, W. Otim-Nape, J. Okello-Onen, C.
943 Rubaire-Akiiki, J. Konde-Lule, and S. Ogwal-Byenek, 2013: Nature and dynamics of
944 climate variability in the Uganda cattle corridor. *Afr. J. Environ. Sci. Tech.,* **7**, 770-782,
945 https://doi.org/10.5897/AJEST2013.1435

946 Otte, I., F. Detsch, E. Mwangomo, A. Hemp, T. Appelhans, and T. Nauss, 2017: Multidecadal
947 trends and interannual variability of rainfall as observed from five lowland stations at Mt.
948 Kilimanjaro, Tanzania. *J. Hydrometeor.,* **18**, 349-361, https://doi.org/10.1175/JHM-D-
949 16-0062.1

950 Palmer, P. I., and Coauthors, 2023: Drivers and impacts of Eastern African rainfall variability.
951 *Nat. Rev. Earth Environ.,* **4**, 254-270, https://doi.org/10.1038/s43017-023-00397-x

952 Panthou, G., and Coauthors, 2018: Rainfall intensification in tropical semi-arid regions: the
953 Sahelian case. *Environ. Res. Lett*, ***13***, 064013, https://doi.org/10.1088/1748-9326/aac334

954 Pausata, F. S., M. Gaetani, G. Messori, A. Berg, D. M. de Souza, R. F. Sage, P. B. deMenocal,
955 2020: The greening of the Sahara: Past changes and future implications. *One Earth,* **2**,
956 235-250, https://doi.org/10.1016/j.oneear.2020.03.002

957 RRC, 2023: Flood assessment report in South Sudan. Accessed 7 May 2025,
958 https://www.undp.org/south-sudan/publications/flood-assessment-report-south-sudan

959 Rowell, D. P., B. B. Booth, S. E. Nicholson, and P. Good, 2015: Reconciling past and future
960 rainfall trends over East Africa. *J. Climate,* **28**, 9768-9788, https://doi.org/10.1175/JCLI-
961 D-15-0140.1

962 Salerno, J., J. E. Diem, B. L. Konecky, and J. Hartter, 2019: Recent intensification of the
963 seasonal rainfall cycle in equatorial Africa revealed by farmer perceptions, satellite-based
964 estimates, and ground-based station measurements. *Climatic Change,* **153**, 123-139,
965 https://doi.org/10.1007/s10584-019-02370-4

966 Sanogo, S., A. H. Fink, J. A. Omotosho, A. Ba, R. Redl, and V. Ermert, 2015: Spatio-temporal
967 characteristics of the recent rainfall recovery in West Africa. *Int. J. Climatol.,* **35**, 4589-
968 4605, https://doi.org/10.1002/joc.4309

969 Schwarzwald, K., L. Goddard, R. Seager, M. Ting, and K. Marvel, 2023a: Understanding
970 CMIP6 biases in the representation of the Greater Horn of Africa long and short rains.

971 *Climate Dyn.,* **61**, 1229-1255, https://doi.org/10.1007/s00382-022-06622-5

972 Schwarzwald, K., and R. Seager, 2024: Revisiting the "East African Paradox": CMIP6 models
973 also struggle to reproduce strong observed Long Rain drying trends. *J. Climate,* **37**, 6641-
974 6658, https://doi.org/10.1175/JCLI-D-24-0225.1

975 Seager, R., M. Cane, N. Henderson, D. E. Lee, R. Abernathey, and H. Zhang, 2019:
976 Strengthening tropical Pacific zonal sea surface temperature gradient consistent with
977 rising greenhouse gases. *Nat. Climate Change,* **9**, 517-522,
978 https://doi.org/10.1038/s41558-019-0505-x

979 Seleshi, Y., and U. Zanke, 2004: Recent changes in rainfall and rainy days in Ethiopia. *Int. J.*
980 *Climatol.,* **24**, 973-983, https://doi.org/10.1002/joc.1052

981 Sen, P. K., 1968: Estimates of the regression coefficient based on Kendall's tau. *J. Amer. Stat.*
982 *Assoc.,* **63**, 1379-1389, https://doi.org/10.1080/01621459.1968.10480934

983 Seregina, L. S., A. H. Fink, R. van der Linden, N. A. Elagib, and J. G. Pinto, 2019: A new and
984 flexible rainy season definition: Validation for the Greater Horn of Africa and application
985 to rainfall trends. *Int. J. Climatol.,* **39**, 989-1012, https://doi.org/10.1002/joc.5856

986 Sun, S., Y. Fang, Y. Zu, L. Liu, and K. Li, 2022: Increased occurrences of early Indian Ocean
987 Dipole under global warming. *Sci. Adv.,* **8**, eadd6025,
988 https://doi.org/10.1126/sciadv.add6025

989 Taylor, R. G., M. C. Todd, L. Kongola, L. Maurice, E. Nahozya, H. Sanga, and A. M.
990 MacDonald, 2013: Evidence of the dependence of groundwater resources on extreme
991 rainfall in East Africa. *Nat. Climate Change*, **3**, 374–378,
992 https://doi.org/10.1038/nclimate1731

993 Theil, H., 1950: A rank-invariant method of linear and polynomial regression analysis, Part I;
994 Confidence regions for the parameters of polynomial regression equations. *Proc. Roy.*
995 *Neth. Acad. Sci.,* **53**, 345-381.

996 Verdin, J., C. Funk, G. Senay, and R. Choularton, 2005: Climate science and famine early
997 warning. *Phil. Trans. Roy. Soc. B.,* **360** 2155-2168,
998 https://doi.org/10.1098/rstb.2005.1754

999 Wainwright, C. M., E. Black, and R. P. Allan, 2021b: Future changes in wet and dry season
1000 characteristics in CMIP5 and CMIP6 simulations. *J Hydrometeorol.,* **22**, 2339-2357,
1001 https://doi.org/10.1175/JHM-D-21-0017.1

1002 Wainwright, C. M., D. L. Finney, M. Kilavi, E. Black, and J. H. Marsham, 2020: Extreme
1003 rainfall in East Africa, October 2019-January 2020 and context under future climate
1004 change. *Weather,* **76**, 26-31, https://doi.org/10.1002/wea.3824

1005 Wainwright, C. M., J. H. Marsham, R. J. Keane, D. P. Rowell, D. L. Finney, E. Black, and R.
1006 P. Allan, 2019: 'Eastern African Paradox' rainfall decline due to shorter not less intense
1007 Long Rains. *npj Climate Atmos. Sci.,* **2**, 34, https://doi.org/10.1038/s41612-019-0091-7

1008 Wainwright, C. M., J. H. Marsham, D. P. Rowell, D. L. Finney, and E. Black, 2021a: Future
1009 changes in seasonality in East Africa from regional simulations with explicit and
1010 parameterized convection. *J. Climate*, **34**, 1367-1385, https://doi.org/10.1175/JCLI-D-
1011 20-0450.1

1012 Williams, A. P., and C. Funk, 2011: A westward extension of the warm pool leads to a
1013 westward extension of the Walker circulation, drying eastern Africa. *Climate Dyn.,* **37**,
1014 2417-2435, https://doi.org/10.1007/s00382-010-0984-y

1015 Yang, W., R. Seager, M. A. Cane, and B. Lyon, 2014: The East African long rains in
1016 observations and models. *J. Climate*, ***27***, 7185-7202, https://doi.org/10.1175/jcli-d-13-
1017 00447.1

1018 Yang, W., R. Seager, M. A. Cane, and B. Lyon, 2015: The annual cycle of East African
1019 precipitation. *J. Climate,* **28**, 2385-2404, https://doi.org/10.1175/JCLI-D-14-00484.1

1020 Yvonne, M., G. Ouma, D. Olago, and M. Opondo, 2020: Trends in climate variables
1021 (temperature and rainfall) and local perceptions of climate change in Lamu, Kenya.
1022 *Geogr. Environ. Sustainability,* **13**, 102-109, https://DOI-10.24057/2071-9388-2020-24